Electronic Supplementary Material (ESI) for Nanoscale Advances.

Electronic Supplementary Information

Engineering doping-vacancy double defects and insights into the conversion mechanisms of an Mn-O-F ultrafine nanowire anode for enhanced Li/Na-ion storage and hybrid capacitors

Yongfa Huang, Rui Ding,* Danfeng Ying, Wei Shi, Yuxi Huang, Caini Tan, Xiujuan Sun, Ping Gao, and Enhui Liu

Key Laboratory of Environmentally Friendly Chemistry and Applications of Ministry of Education, College of Chemistry, Xiangtan University, Hunan 411105, P.R. China

*E-mails: drm8122@163.com; drm8122@xtu.edu.cn

Table of Contents

Experimental

Figure S18 The equivalent circuit model of Nyquist plots for MnF_2 and MnF_2 8#-E electrodes.

Figure S19 Nyquist plots of MnF_2 and MnF_2 8#-E electrodes (the insets are the enlarged high frequency regions).

Figure S20 GCD curves of MnF_2 8# (A) and MnF_2 8#-E (B) electrodes at the precharged current density of 0.1 A g^{-1} .

Figure S21 Performance of AC electrode for Li-ion storage.

Figure S22 CV plots at 40 mV s^{-1} (A), GCD curves at 1 A g^{-1} (B), Ragone plots (C) and cycling behavior for 5000 cycles at 5 A g^{-1} (D) of 4.5 V-MnF_2//AC LICs (1:1) and 4.6 V-MnF_2//AC LICs (1:2).

Figure S23 The third cycle of CV curves under 0-5 V at 1 mV s^{-1}: MnF_2//AC LICs (1:1) (A), MnF_2//AC LICs (1:2) (B).

Figure S24 CV plots of 4.5 V-MnF_2//AC LICs (1:1) at 10-160 mV s^{-1} (A), GCD curves of 4.5 V-MnF_2//AC LICs (1:1) at 0.5-16 A g^{-1} (B), CV plots of 4.6 V-MnF_2//AC LICs (1:2) at 10-160 mV s^{-1} (C), GCD curves of 4.6 V-MnF_2//AC LICs (1:2) at 0.5-16 A g^{-1} (D).

Figure S25 CV plots at 40 mV s^{-1} (A), GCD curves at 1 A g^{-1} (B), Ragone plots (C) and cycling behavior for 5000 cycles at 5 A g^{-1} (D) of 4 V-MnF_2//AC LICs (1:1), (1:2) and (1:3).

Figure S26 CV plots of 4 V-MnF_2-E//AC LICs (1:1) (A), 4 V-MnF_2-E//AC LICs (1:2) (C) and 4 V-MnF_2-E/AC LICs (1:3) (E) at 10-160 mV s^{-1}, GCD curves of 4 V-MnF_2-E//AC LICs (1:1) (B), 4 V-MnF_2-E//AC LICs (1:2) (D) and 4 V-MnF_2-E/AC LICs (1:3) (F) at 0.5-16 A g^{-1}.

Figure S27 CV plots of 4 V-MnF_2//AC LICs (1:1) (A) and 4.3 V-MnF_2//AC LICs (1:1) (C) at 10-160 mV s^{-1}, GCD curves of 4 V-MnF_2//AC LICs (1:1) (B) and 4.3 V-MnF_2//AC LICs (1:1) (D) at 0.5-16 A g^{-1}.

Figure S28 CV plots of 4.3 V-MnF_2-E//AC LICs (1:2) (A), GCD curves of 4.3 V-MnF_2-E//AC LICs (1:2) (B) at 0.5-16 A g^{-1}.

Figure S29 GCD curves of MnF_2 8# (A) and MnF_2 8#-E(B) at 0.1-1.6 A g^{-1}.

Figure S30 Rate performance and Coulombic efficiency of MnF_2 8# (A) and MnF_2 8#-E (B) electrodes at 0.1-1.6-0.1 A g^{-1}, Cycling stability and Coulombic efficiency of MnF_2 8# (C) and MnF_2 8#-E (D) electrodes at 0.3 A g^{-1} for 500 cycles.

Figure S31 XRD patterns and TEM images of the MnF_2 8# (A, C, E) and MnF_2 8#-E (B, D, F) electrodes after the cycling for Na-ion storage.

Figure S32 The pseudocapacitive contributions (the shaded region) of the MnF_2 8# electrode at 0.1-0.3 mV s^{-1} (a-c) and the contribution ratios (d) for Na-ion storage.

Figure S33 The pseudocapacitive contributions (the shaded region) of the MnF_2 8#-E electrode at 0.1-0.3 mV s^{-1} (a-c) and the contribution ratios (d) for Na-ion storage.

Figure S34 Nyquist plots of MnF_2 and MnF_2 8#-E electrodes (the insets are the enlarged high frequency regions).

Figure S35 GCD curves of MnF_2 8# (A) and MnF_2 8#-E (B) electrodes at the precharged current density of 0.1 A g^{-1}

Figure S36 Performance of AC electrode for Na-ion storage.

Figure S37 CV plots at 40 mV s^{-1} (A), GCD curves at 1 A g^{-1} (B), Ragone plots (C) and cycling behavior for 5000 cycles at 3 A g^{-1} (D) of 4.6 V-MnF_2//AC NICs (1:1) and 4.8 V-MnF_2//AC NICs (1:2).

Figure S38 The third cycle CV curves at 1 mV s^{-1} under 0-5 V: MnF_2//AC NICs (1:1) (A), and MnF_2//AC NICs (1:2) (B).

Figure S39 CV plots of 4.6 V-MnF_2//AC NICs (1:1) (A) and 4.8 V-MnF_2//AC NIC (1:2) (C), at 10-160 mV s^{-1}, GCD curves of 4.6 V-MnF_2//AC NIC (1:1) (B) and 4.8 V-MnF_2//AC NICs (1:2) (D) at 0.5-8 A g^{-1}.

Figure S40 CV plots of 4 V-MnF_2//AC NICs (1:1) (A) and 4.3 V-MnF_2//AC NICs (1:1) (C), at 10-160 mV s^{-1}, GCD curves of 4 V-MnF_2//AC NICs (1:1) (B) and 4.3 V-MnF_2//AC NICs (1:1) (D) at 0.5-8 A g^{-1}.

Figure S41 CV plots of 4 V-MnF_2-E//AC NICs (1:1) (A) and 4.3 V-MnF_2-E//AC NICs (1:1) (C) at 10-160 mV s^{-1}, GCD curves of 4 V-MnF_2-E//AC NICs (1:1) (B) and 4.3 V-MnF_2-E//AC NICs (1:1) (D) at 0.5-8 A g^{-1}.

Table S1 Orthogonal experimental design.

Table S2 Synthesis condition of MnF_2 1#-9#.

Table S3 Orthogonal experimental analysis results of MnF_2

Table S4 Summary of performance of MnF_2 1#-9# and MnF_2 8#-E electrodes.

Table S5 A comparasion for Mn-O-F (MnF_2 8#-E) anode with literature for LIBs.

Table S6 EIS parameters of MnF_2 and MnF_2 8#-E electrodes for Li-ion storage.

Table S7 Summary of performance of MnF_2//AC and MnF_2-E//AC LICs and NICs.

Table S8 Electrochemical performance comparison for some reported LICs.

Table S9 EIS parameters of MnF_2 8# and MnF_2 8#-E electrodes for Na-ion storage.

Table S10 Electrochemical performance comparison for some reported NICs.

Table S11 Chemicals, agents and materials.

References

Experimental

Synthesis of materials

The MnF_2 materials were synthesized by one-pot solvothermal method according to the orthogonal experiment (**Table S1, S2**). Take the procedure of MnF_2 8# for an example. The compounds of 4 mmol $Mn(CH_3COO)_2\bullet 4H_2O$ and 7 mL HF (40%) were added into 30 mL ethylene glycol (EG) solvents, and the mixture was magnetically stirred thoroughly and dispersed well in an ultrasonic bath. Subsequently, the mixture was put into a 50 ml Teflon lined stainless steel reactor, which was heated at 190 ^{o}C for 6 h in an electric oven, and cooled down naturally. Then, the yielded precipitates were washed with absolute alcohol serveral times and collected by centrifugal filtration. Finally, the collected precipitates were dried overnight at 100 ^{o}C to obtain the ultimate products. The other eight MnF_2 samples were also synthesized as the procedure described above based on the specific orthogonal experiment conditions.

The Mn-O-F (MnF_2 8#-E) materials were synthesized by a simple etching method as follows: 100 mg of MnF_2 8# was added into 1 M $NaBH_4$ aqueous solution with continuous stirring for 1 h, next, the mixture was centrifuged with distilled water and absolute alcohol in turn for several times, and then the precipitates were placed in a drying oven at 100 ℃ for 12 h to obtain the Mn-O-F materials. The possible process for the formation of Mn-O-F ultrafine nanowires can be seen in the **Scheme 1** (ESI) (the chemicals in the experiment can be seen in the **Table S11**).

Characterizations

The phases and crystallinity properties were determined by X-ray diffraction (XRD). The surface chemical compositions and electronic structures were checked by X-ray photoelectron spectra (XPS). The morphology and size of particles were analyzed by scanning electron microscopy (SEM) and transmission electron microscopy (TEM). The crystalline microstructures were resolved by the high-resolution TEM (HRTEM) and selected area electron diffraction (SAED). The element composition and distribution were measured by X-Ray energy dispersive spectra (EDS) and mapping. The chemical functional groups were meaured by Fourier transform infrared spectroscopy (FTIR). The specific surface area, pore volume and size distribution were examined by nitrogen isothermal sorptions with Brunauer-Emmett-Teller (BET) and Barrett-Joyner-Halenda (BJH) methods.

Electrochemical measurements

The electrodes were prepared as follows: firstly, a well-dispersed mixture of 70 wt% active materials (as-synthesized MnF_2 (1#-9# and 8#-E) or commercial activated carbon (AC), 20 wt% AB conductive agent and 10 wt% polyvinylidene fluoride (PVDF) binder dissolved into the N-methyl-2-pyrrolidone (NMP)) were casted onto the current collectors (the collectors for anode and cathode are Cu foil and carbon-coated Al foil respectively, with the thickeness of 15 μm), and followed by drying in a vacuum oven at 110 ^{o}C for 12 h; Secondly, the electrodes were punched into disks with diameter of 12 mm, and the mass loading of active materials was about 1-4 mg cm^{-2}. The electrochemical performances were examined by cyclic voltammetry (CV), galvanostatistic charge/discharge (GCD) and electrochemical impedance spectroscopy (EIS) tests via CHI 660E electrochemical working stations and Neware-CT-4008 testers. Tests for Li//MnF_2 (1#-9# and 8#-E) and Li//AC or Na//MnF_2 (8# and 8#-E) and Na//AC half-cells were conducted by using the type 2032 coin cells with a MnF_2 or AC working electrode (WE), a Li or Na plate as both counter electrode (CE) and reference electrode (RE), and one piece of glass fiber (GF) as separator. Tests for MnF_2 (8# and 8#-E)//AC LICs/NICs full-cells were conducted via type 2032 coin cells, with certain active mass ratio of anode and cathode, and the MnF_2 (8# and 8#-E) anodes were precharged (pre-lithiation or pre-sodiation) at 0.1 A g^{-1} for 3.5 cycles. The electrolytes for Li//MnF_2 (1#-9# and 8#-E) and Li//AC half-cells and MnF_2 (8# and 8#-E)//AC LICs were 1 M $LiPF_6$ dissolved in the mixed solvents of ethylene carbonate (EC), ethyl methyl carbonate (EMC) and dimethyl carbonate (DMC) (1:1:1 in volume) with 1% vinylene carbonate (VC) additives (CAPCHEM); The electrolytes for Na//MnF_2 (8# and 8#-E) and Na//AC half-cells and MnF_2 (8# and 8#-E)//AC NICs were 0.85 M $NaPF_6$ dissolved in the mixed solvents of EC, and dimethyl carbonate (DEC) (1:1 in volume) with 5% fluoroethylene carbonate (FEC) additives (MJS). All cell assemblies were performed in an high pure Ar-filled dry glovebox (MIKROUNA, O_2 and H_2O<0.1 ppm), and all tests were carried out at room temperature (about 25 ^{o}C). The chemicals, agents and materials for electrochemical tests are listed in the **Table S11**. The calculations for the specific capacity (C_m, mAh g^{-1}), energy density (E_m, Wh kg^{-1}) and power density (P_m, kW kg^{-1}) are on the basis of **Equations S(1), (2) and (3)**:

$$C_m=Q/3.6m \qquad S(1)$$

$$E_m=(C_m \triangle V)/2 \qquad S(2)$$

$$P_m=3.6E_m/t \qquad S(3)$$

Where m, Q, $\triangle V$, and t are mass of active materials (g, for LICs and NICs, it refers to the total masses of active materials of anode and cathode), charge quantity (C), voltage window (V), and discharge time (s), respectively.

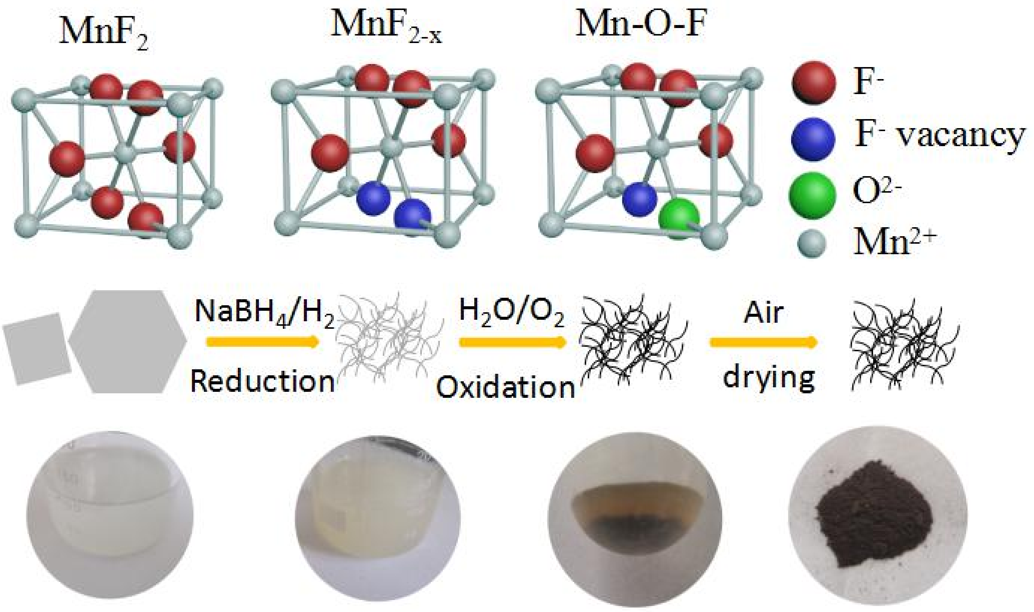

Scheme S1 Schematics of the process for the formation of Mn-O-F ultrafine nanowires.

The possible process for the formation of Mn-O-F ultrafine nanowires can be seen in the **Scheme 1** (ESI). In the etching process by $NaBH_4$ solutions, the bonds among crystalline particles would be weakened and the crystals would become more porous and linear and finally form nanowire morphology under the continuous impact of H_2 flow, meanwhile, the Mn^{2+} would be partially reduced to unstable Mn^{+} in the MnF_2 nanocrystal and produce the F^- vacancy; during the centrifugal filtration, with the removal of the excess of $NaBH_4$ solutions, the unstable Mn^{+} in the MnF_2 nanocrystal would be oxidized to stable Mn^{2+} by O_2 in air and the O^{2-} would also partially occupy the position of F^- vacancy and finally form the Mn-O-F nanowires with the hetero oxygen doping and fluorine vacancies double defects.

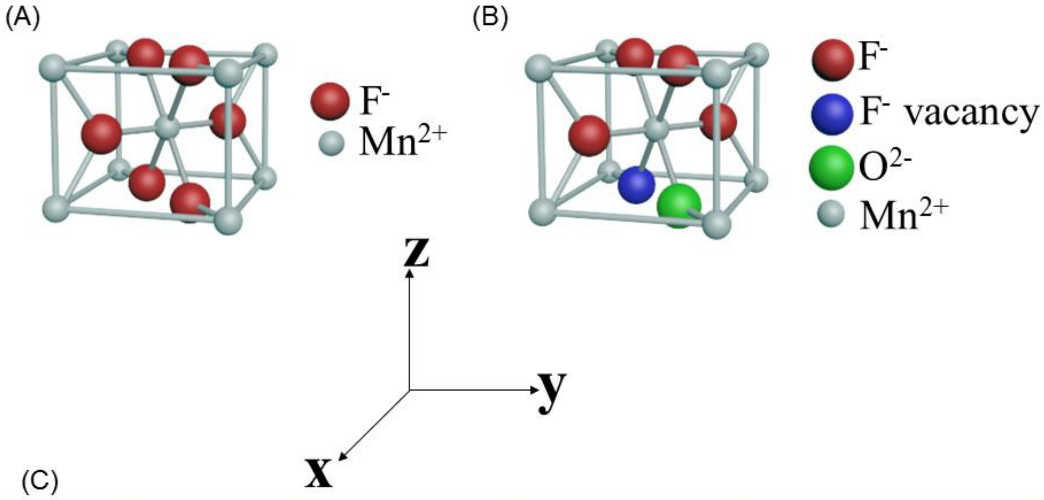

(C)

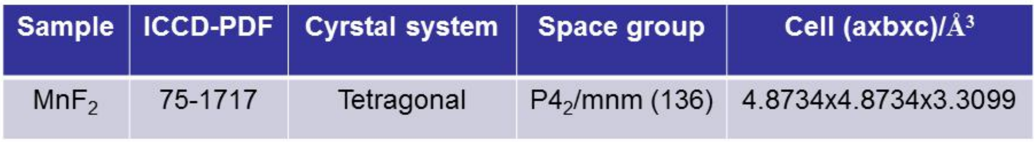

Sample	ICCD-PDF	Cyrstal system	Space group	Cell (axbxc)/Å^3
MnF$_2$	75-1717	Tetragonal	P4$_2$/mnm (136)	4.8734x4.8734x3.3099

Figure S1 The crystal structures of tetragonal MnF$_2$ (A) and defective MnF$_2$-E (B) and detailed crystalline parameters for tetragonal MnF$_2$ (C).

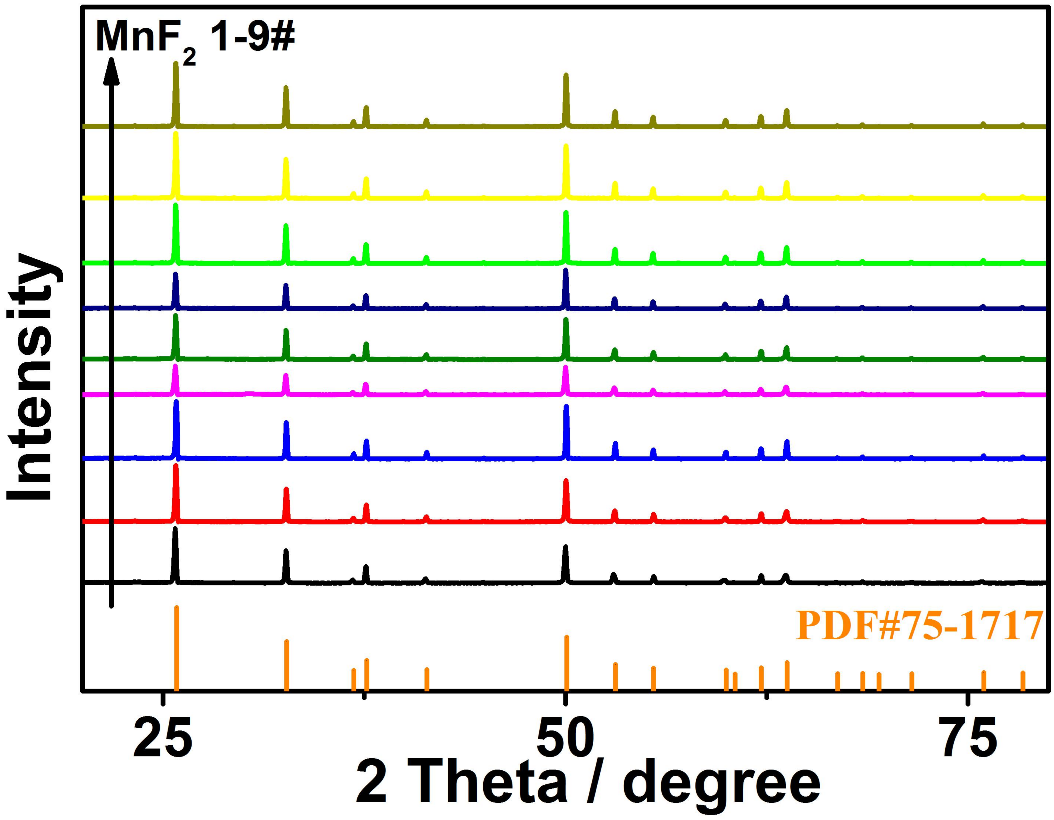

Figure S2 XRD patterns of MnF$_2$ 1#-9# samples.

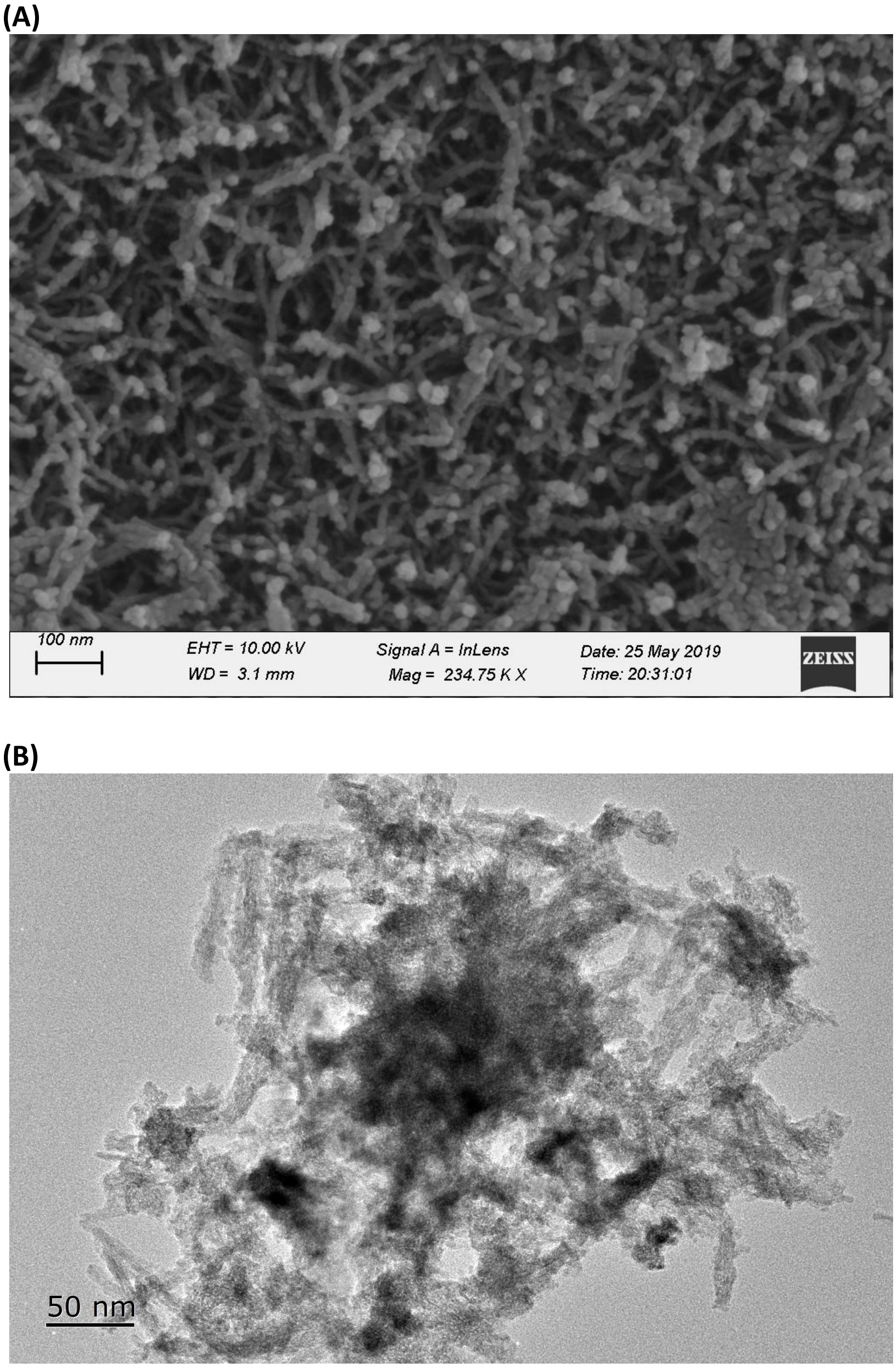

Figure S3 SEM (A)/TEM (B) images of MnF_2 8#-E sample.

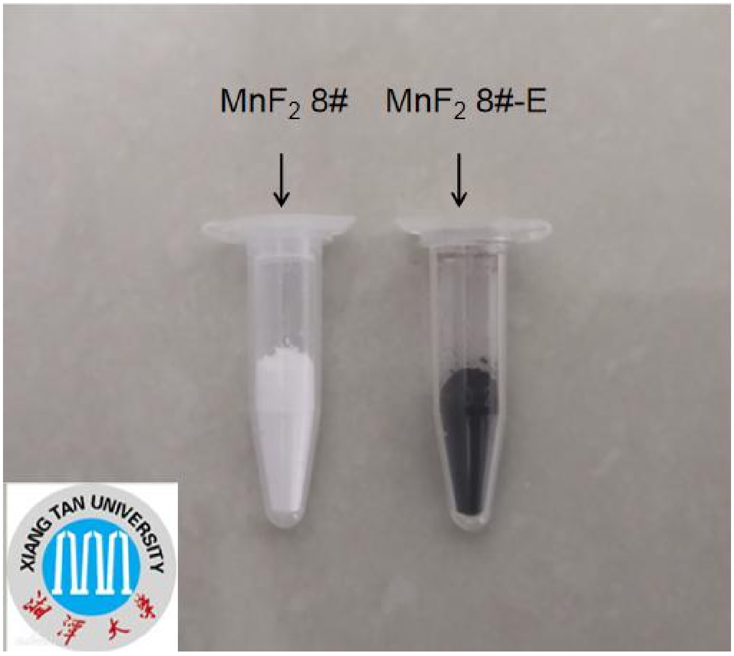

Figure S4 A picture of MnF_2 8# and MnF_2 8#-E samples.

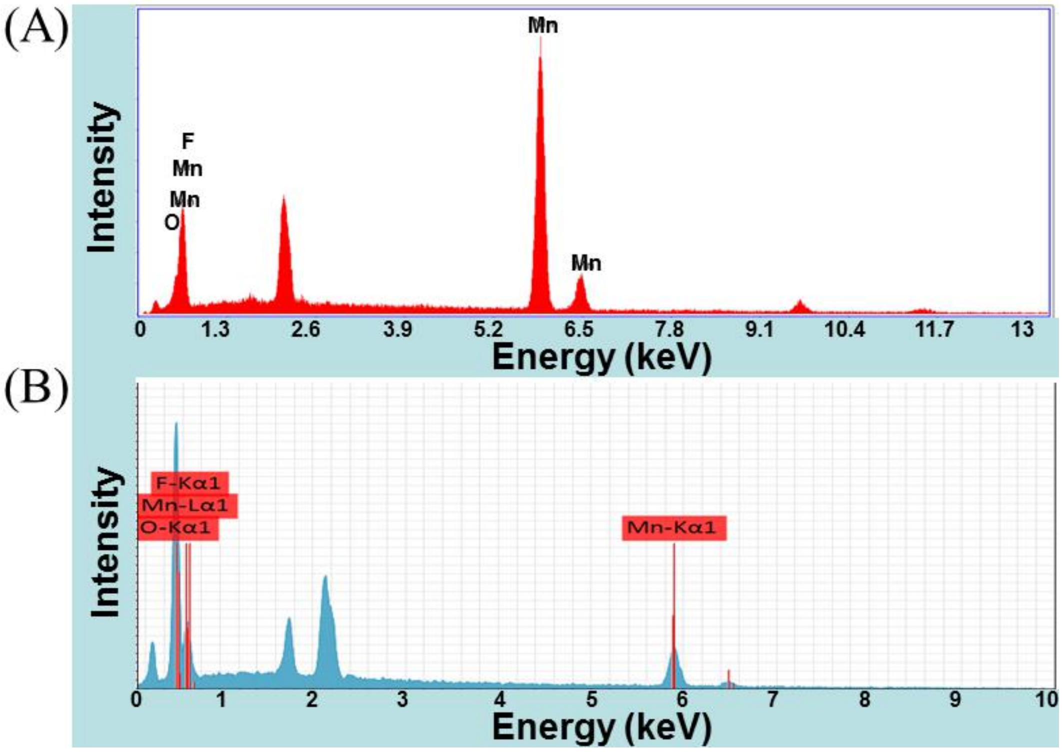

Figure S5 EDS spectra of MnF_2 8# (A) and MnF_2 8#-E (B) samples.

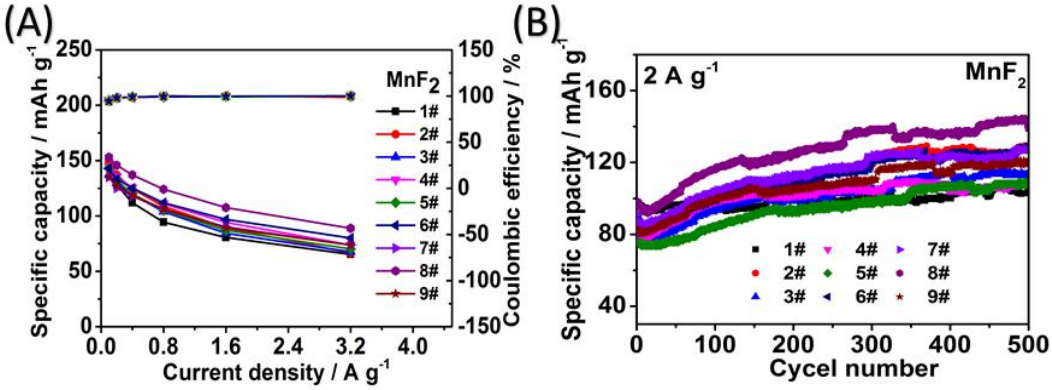

Figure S6 Specific capacity and Coulombic efficiency derived from the respective 5th cycle at 0.1-3.2 A g $^{-1}$ of MnF_2 1#-9# electrodes (A); cycling stability for 500 cycles at 2 A g $^{-1}$ of MnF_2 1#-9# electrodes (B).

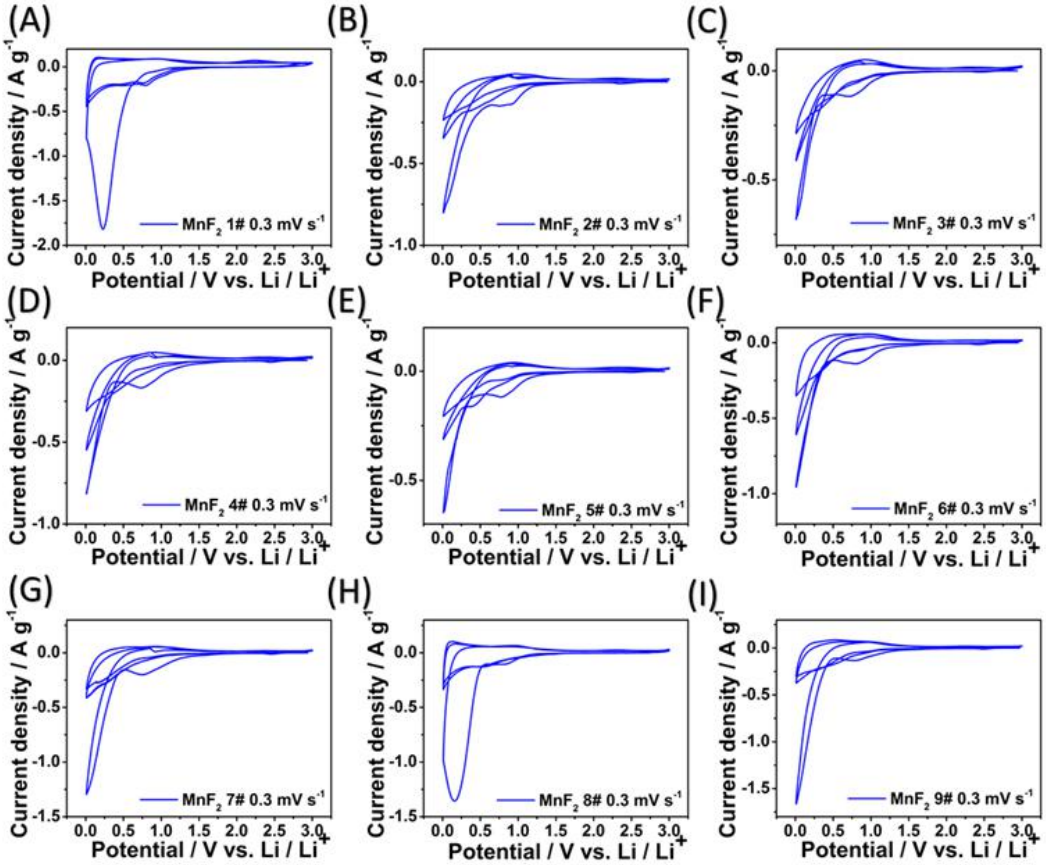

Figure S7 CV plots of the first three cycles of MnF$_2$ 1#-9# electrodes at 0.3 mV s^{-1}.

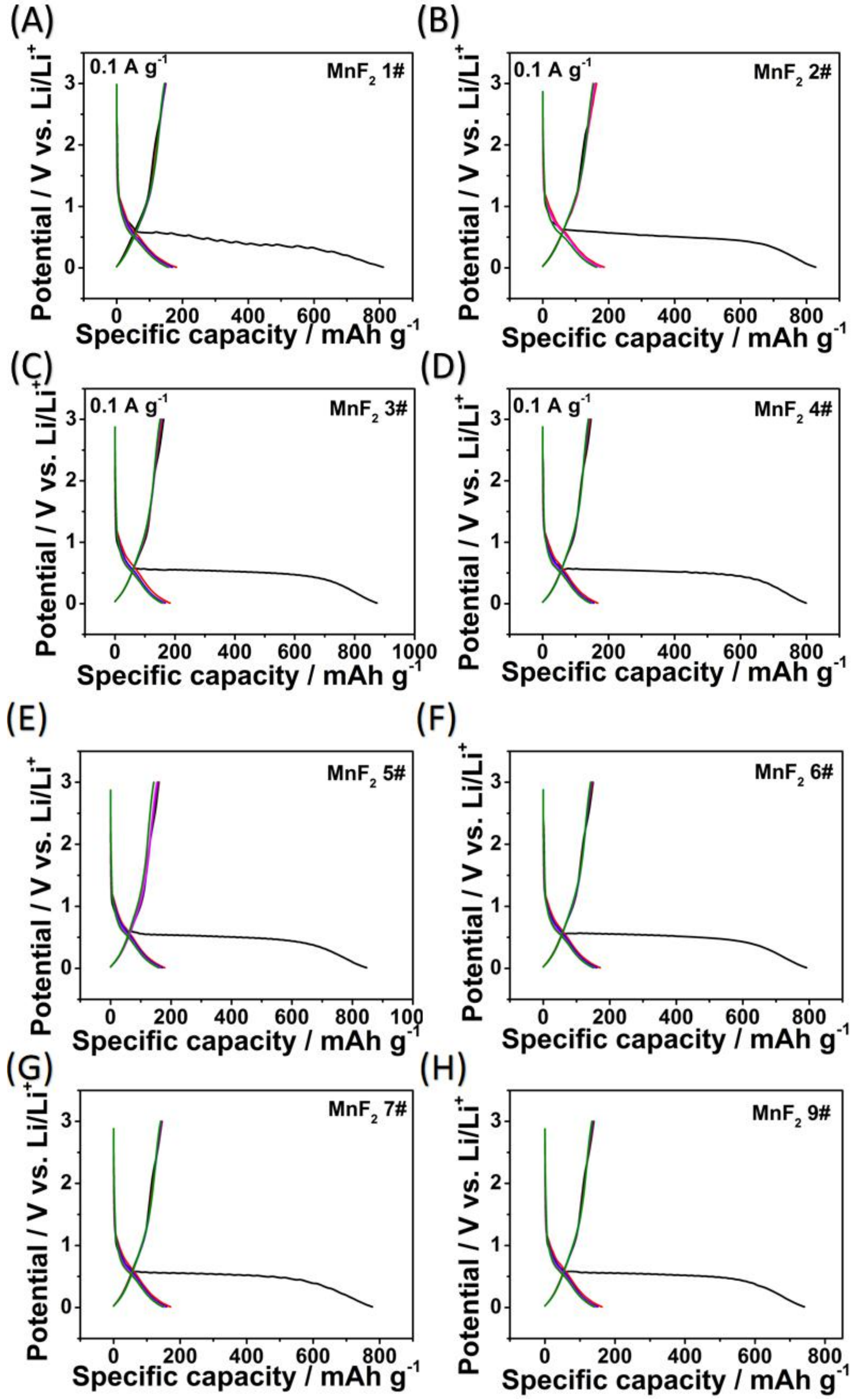

Figure S8 GCD curves of the first five cycles for MnF_2 (1#, 2#, 3#, 4#, 5#, 6#, 7#, 9#) electrodes at 0.1 A g^{-1}.

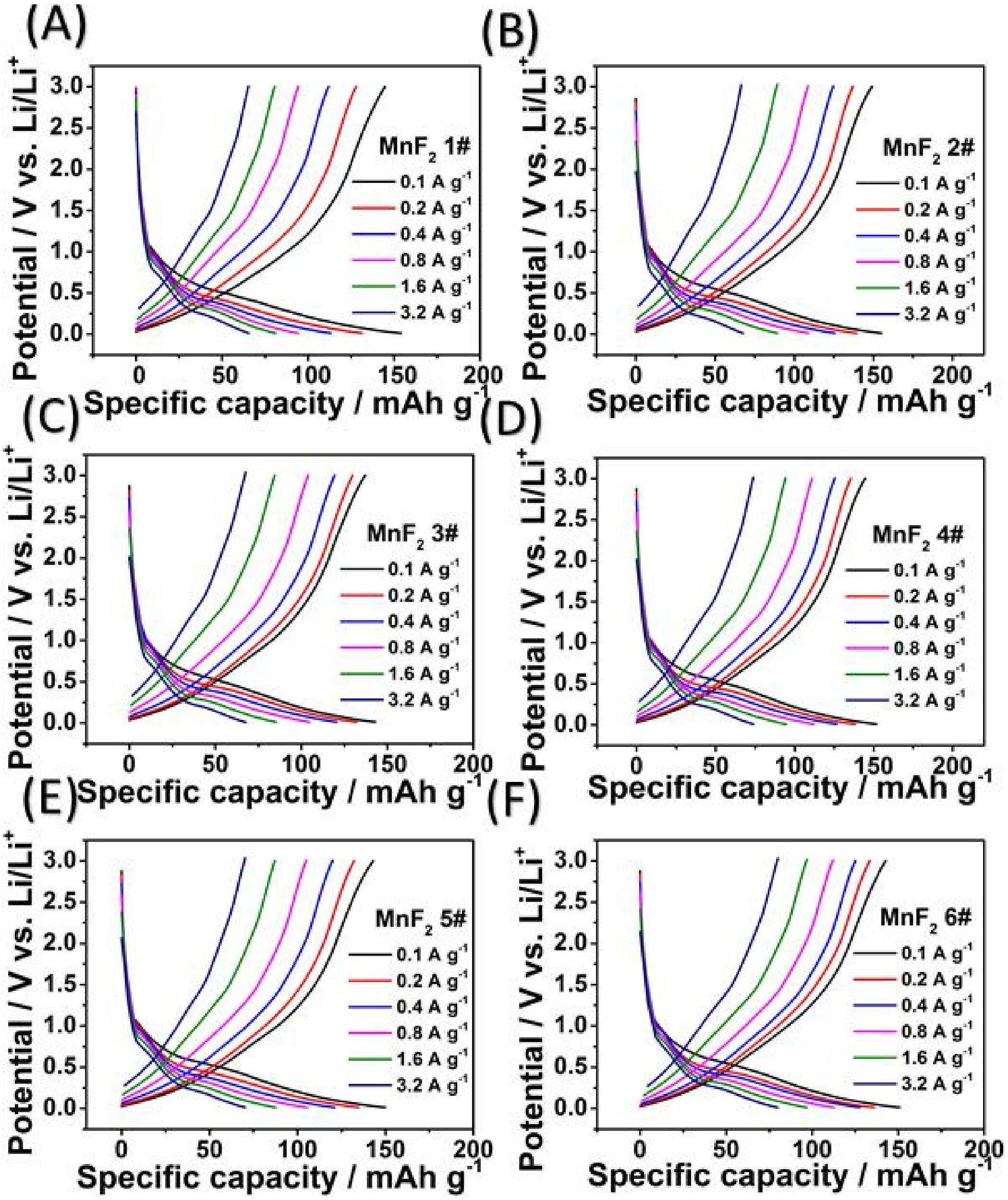

Figure S9 GCD curves of MnF$_2$ 1#-6# electrodes at 0.1-3.2 A g^{-1}.

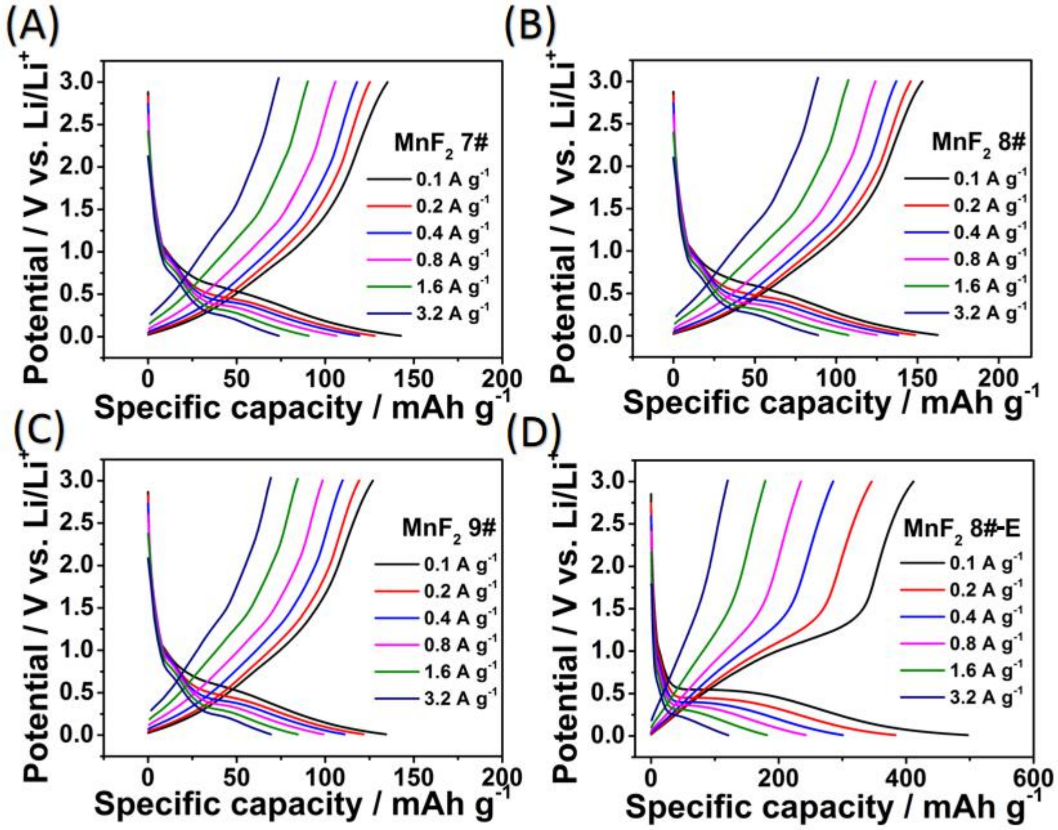

Figure S10 GCD curves of MnF$_2$ 7#-9# and MnF$_2$ 8#-E electrodes at 0.1-3.2 A g^{-1}.

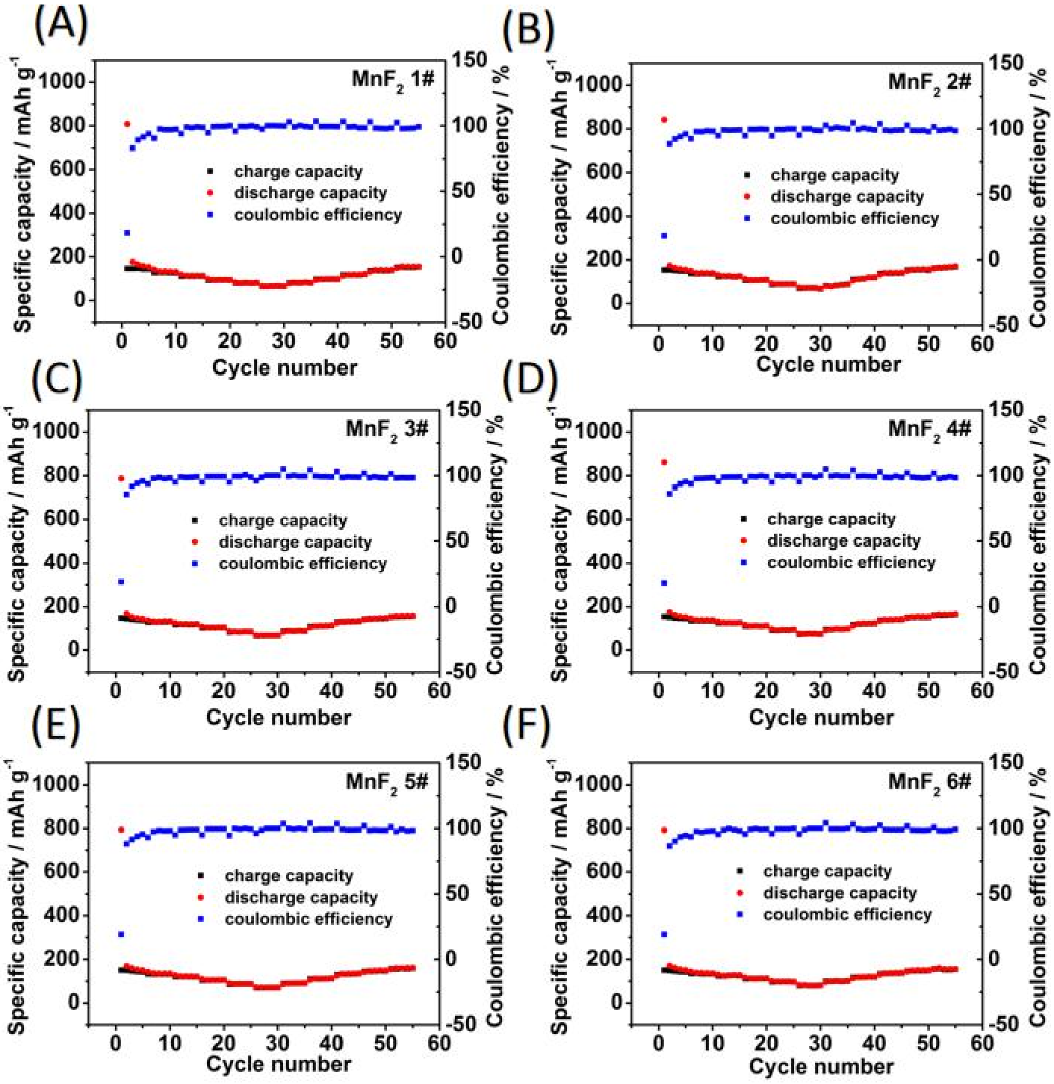

Figure S11 Rate performance and Coulombic efficiency of MnF$_2$ 1#-6# electrodes at 0.1-3.2-0.1 A g^{-1}.

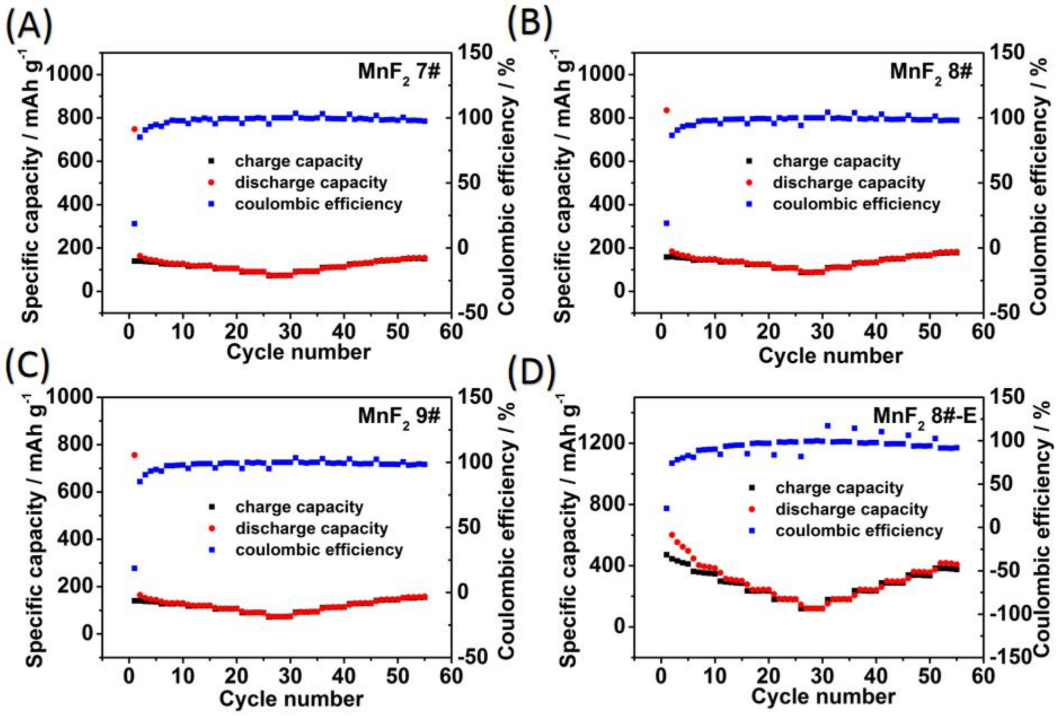

Figure S12 Rate performance and Coulombic efficiency of MnF$_2$ 7#-9# and MnF$_2$ 8#-E electrodes at 0.1-3.2-0.1 A g^{-1} .

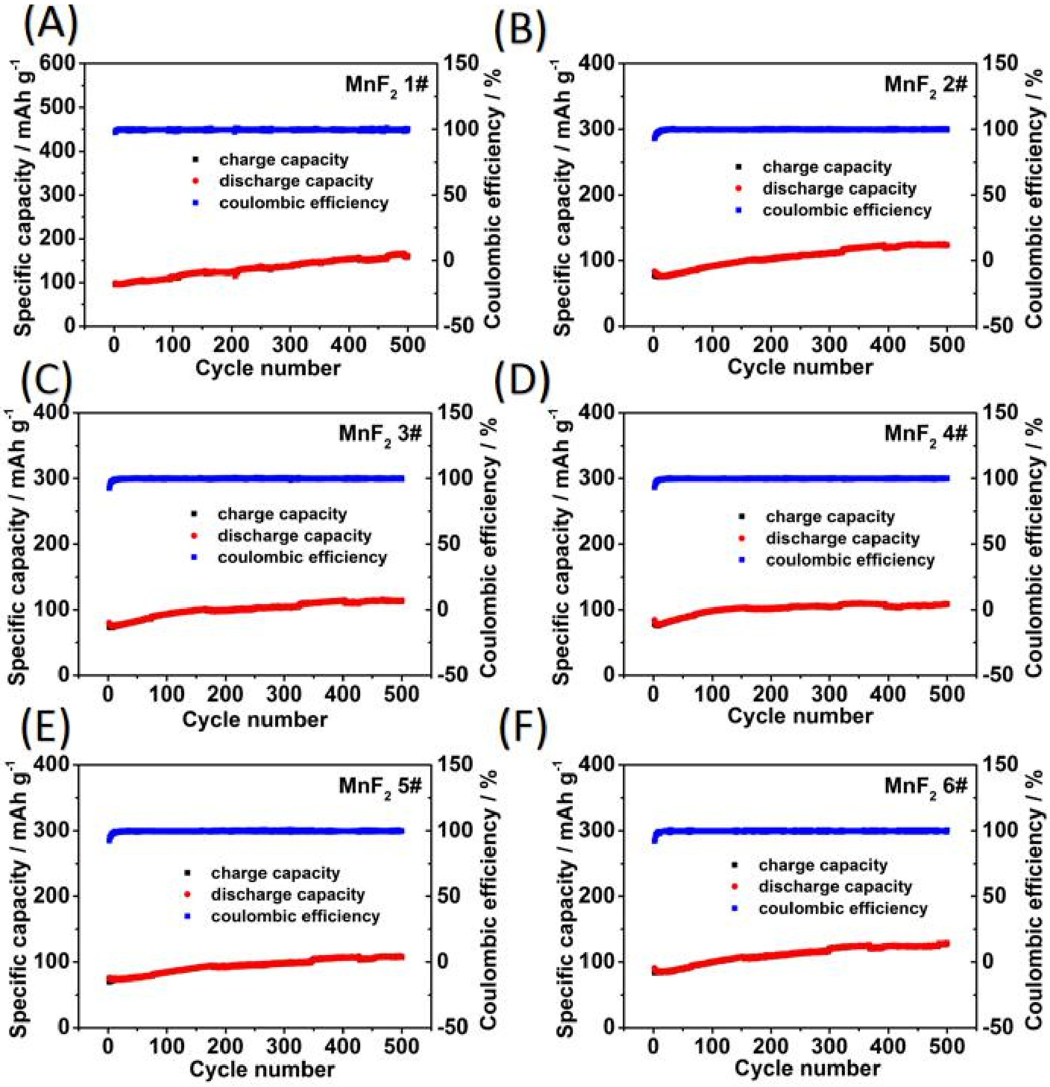

Figure S13 Cycling stability and Coulombic efficiency of MnF_2 1#-6# electrodes at 2 A g^{-1} for 500 cycles.

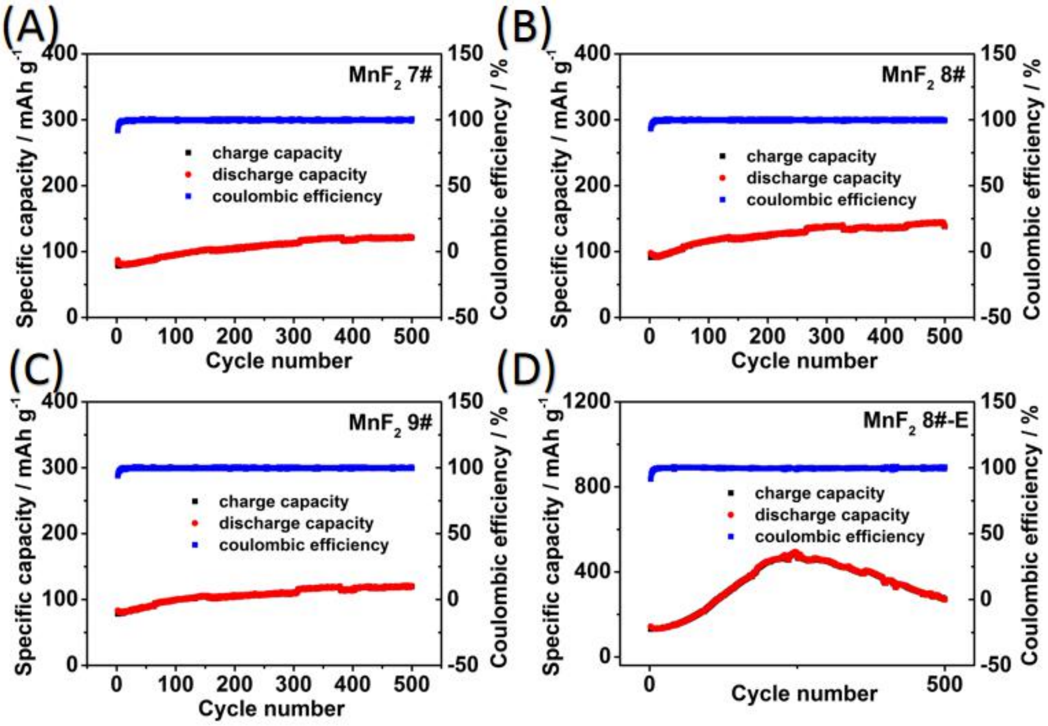

Figure S14 Cycling stability and efficiency efficiency of MnF_2 7#-9# and MnF_2 8#-E electrodes at 2 A g^{-1} for 500 cycles.

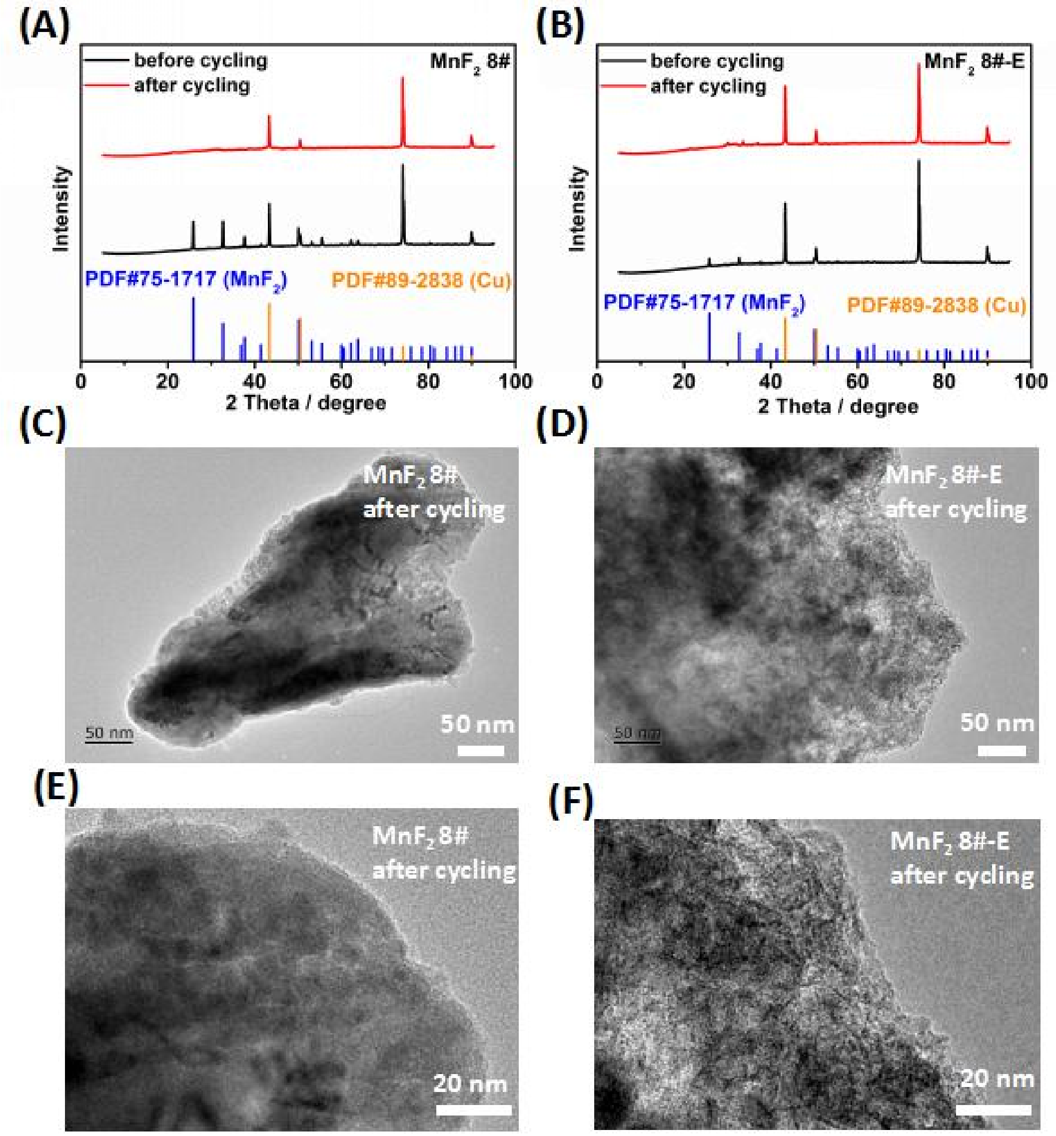

Figure S15 XRD patterns and TEM images of the MnF_2 8# (A, C, E) and MnF_2 8#-E (B, D, F) electrodes after the cycling for Li-ion storage.

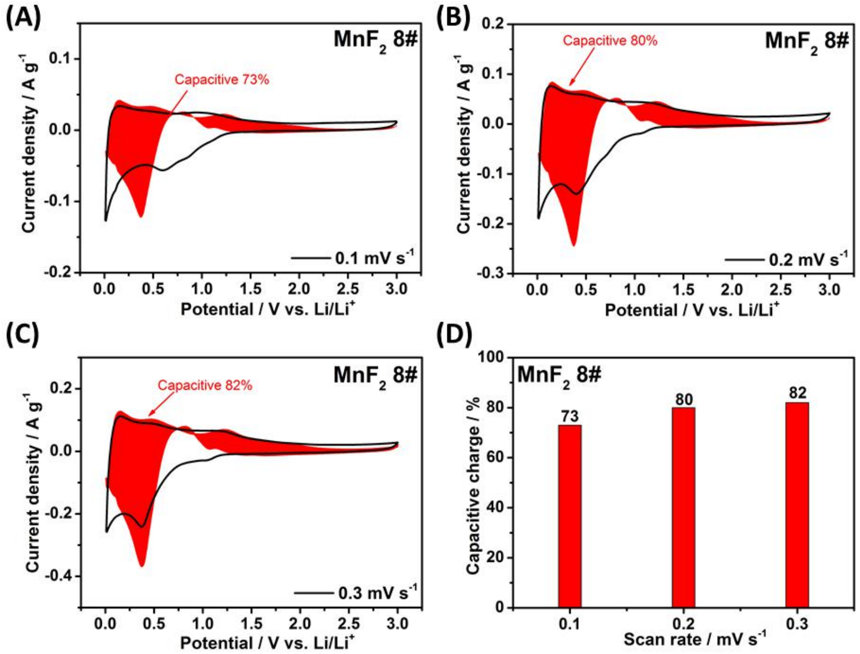

Figure S16 The pseudocapacitive contributions (the shaded region) of the MnF_2 8# electrode at 0.1-0.3 mV s^{-1} (a-c) and the contribution ratios (d) for Li-ion storage.

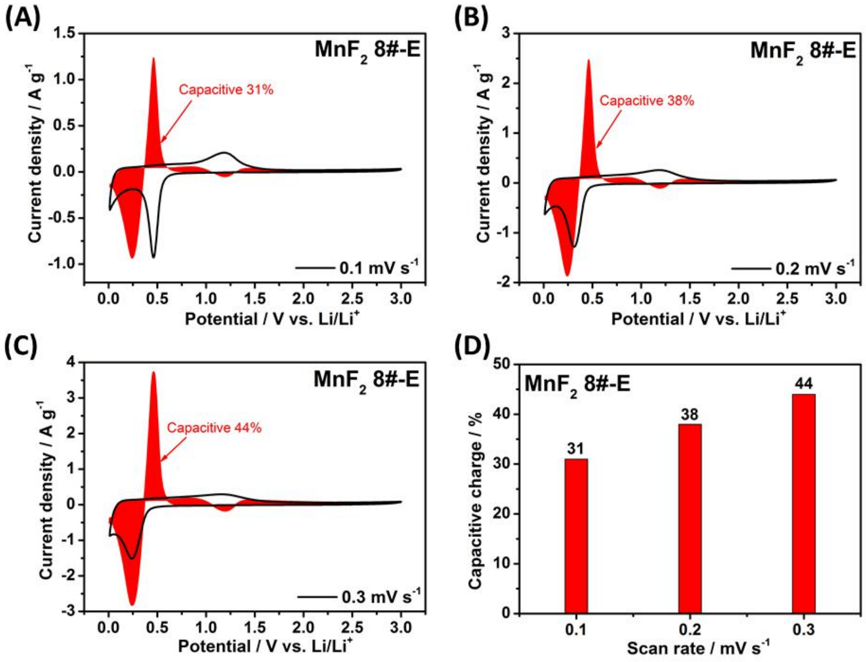

Figure S17 The pseudocapacitive contributions (the shaded region) of the MnF_2 8#-E electrode at 0.1-0.3 mV s^{-1} (a-c) and the contribution ratios (d) for Li-ion storage.

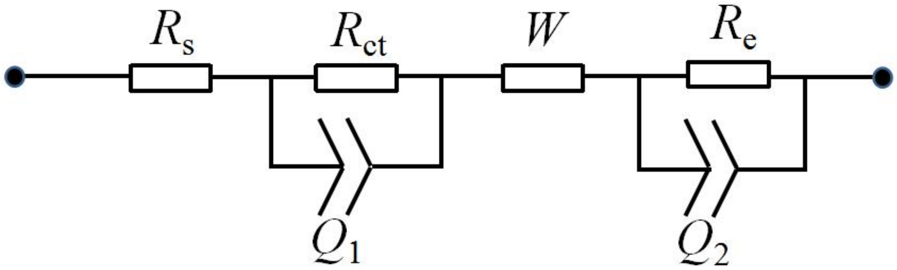

Figure S18 The equivalent circuit model of Nyquist plots for MnF_2 and MnF_2 8#-E electrodes.

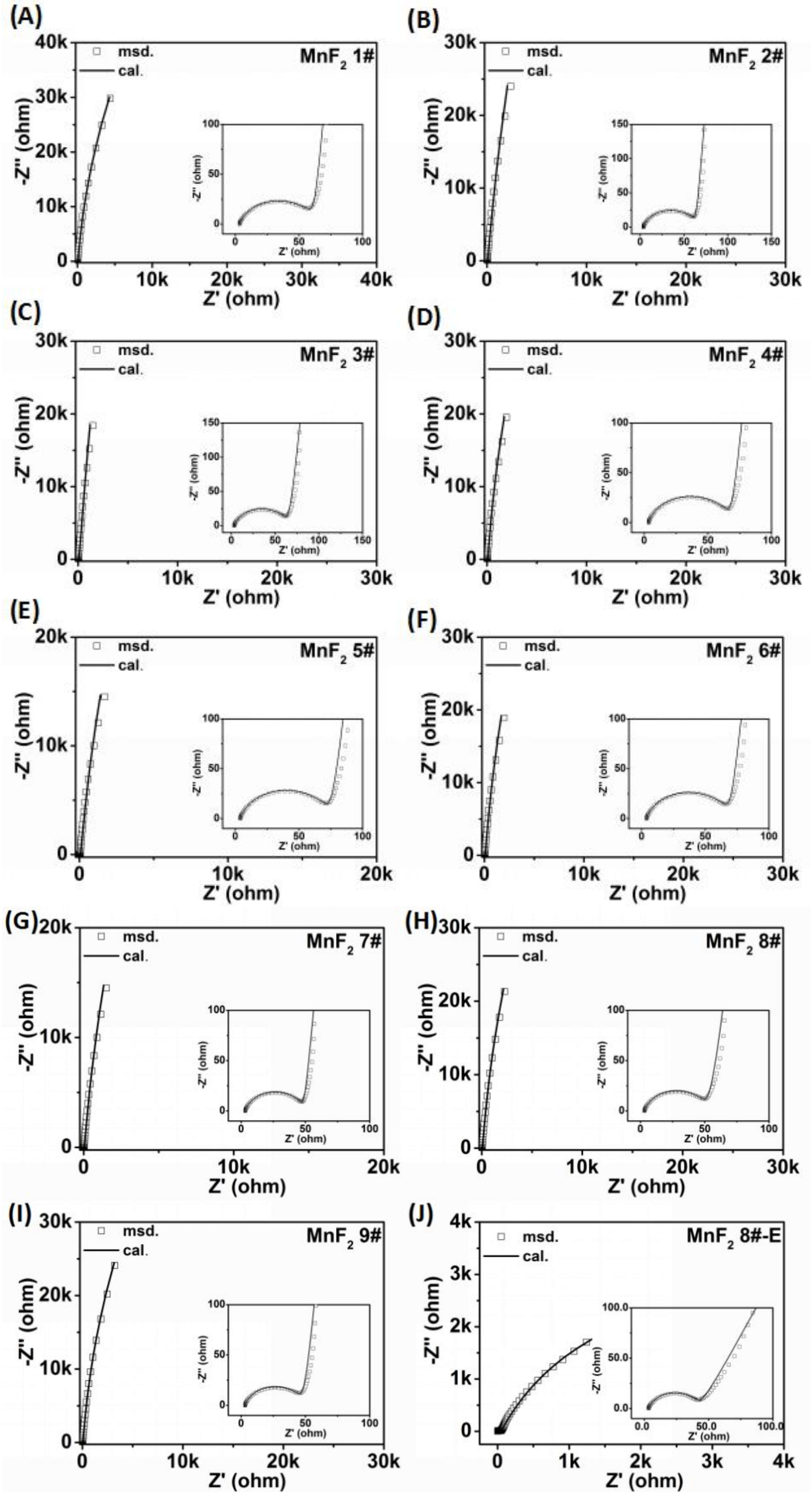

Figure S19 Nyquist plots of MnF$_2$ and MnF$_2$ 8#-E electrodes (the insets are the enlarged high frequency regions).

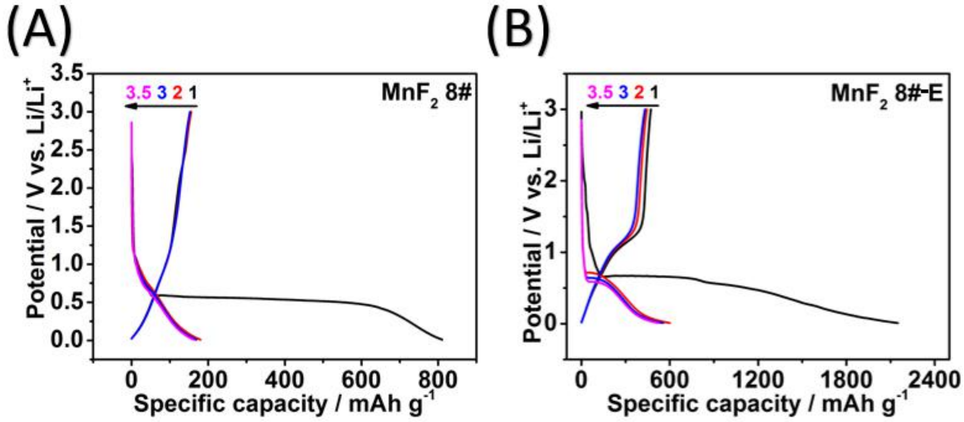

Figure S20 GCD curves of MnF$_2$ 8# (A) and MnF$_2$ 8#-E (B) electrodes at the precharged current density of 0.1 A g^{-1} .

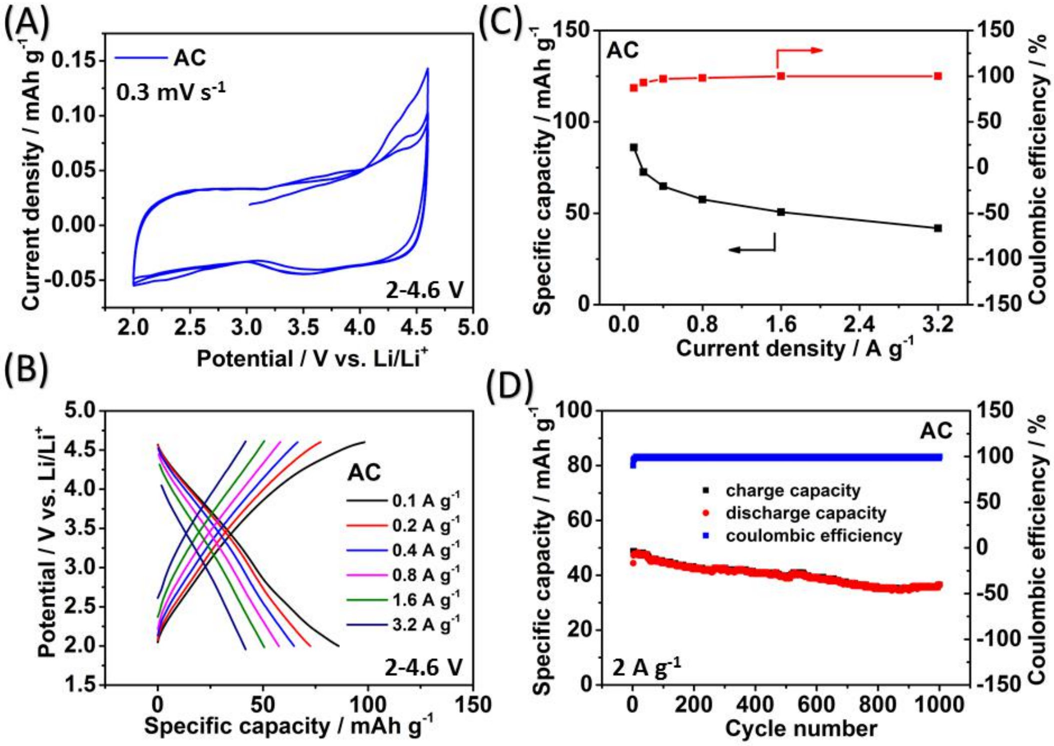

Figure S21 Performance of AC electrode for Li-ion storage.

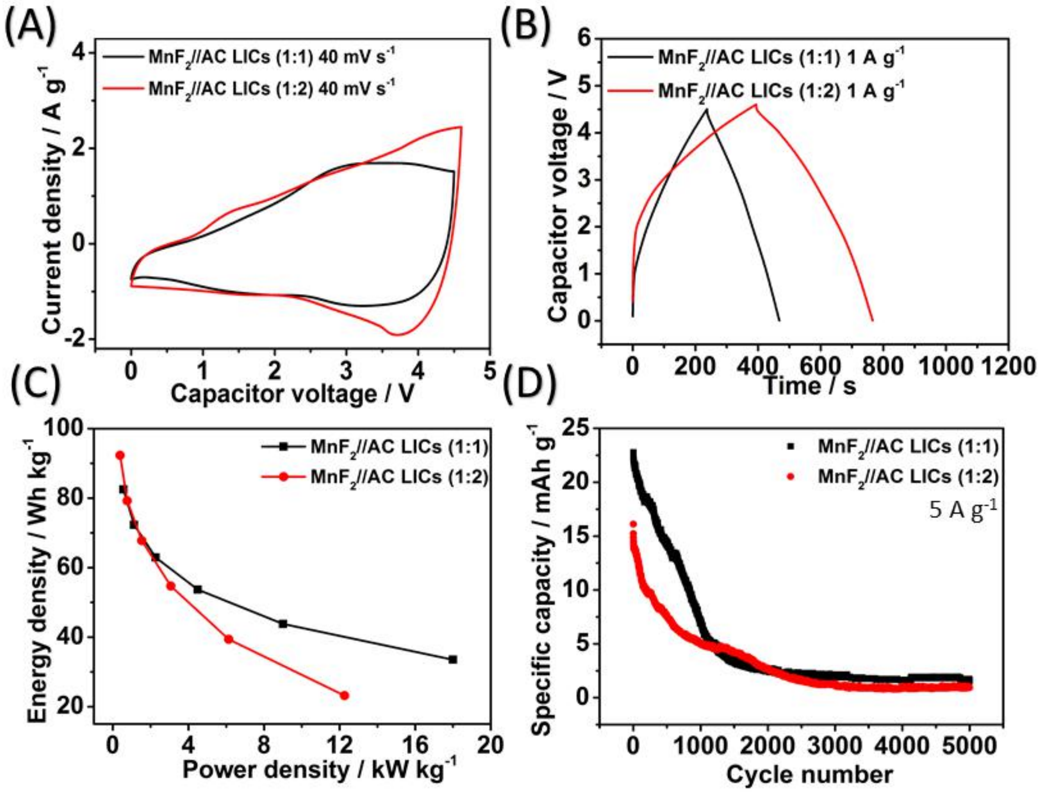

Figure S22 CV plots at 40 mV s^{-1} (A), GCD curves at 1 A g^{-1} (B), Ragone plots (C) and cycling behavior for 5000 cycles at 5 A g^{-1} (D) of 4.5 V-MnF$_2$//AC LICs (1:1) and 4.6 V-MnF$_2$//AC LICs (1:2).

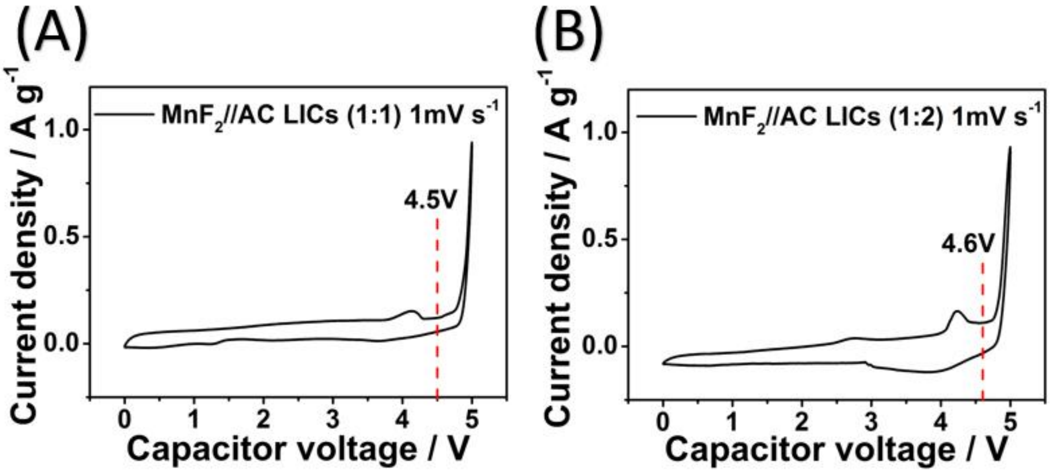

Figure S23 The third cycle of CV curves under 0-5 V at 1 mV s^{-1}: MnF_2//AC LICs (1:1) (A), MnF_2//AC LICs (1:2) (B).

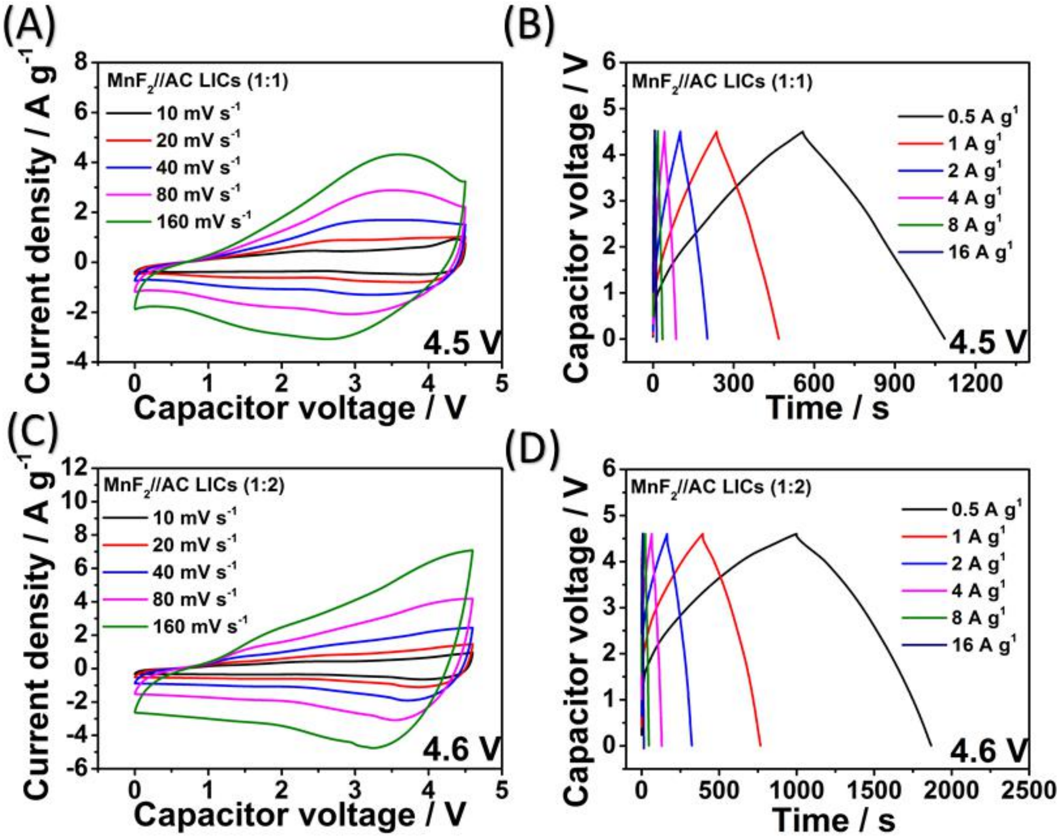

Figure S24 CV plots of 4.5 V-MnF$_2$//AC LICs (1:1) at 10-160 mV s^{-1} (A), GCD curves of 4.5 V-MnF$_2$//AC LICs (1:1) at 0.5-16 A g^{-1} (B), CV plots of 4.6 V-MnF$_2$//AC LICs (1:2) at 10-160 mV s^{-1} (C), GCD curves of 4.6 V-MnF$_2$//AC LICs (1:2) at 0.5-16 A g^{-1} (D).

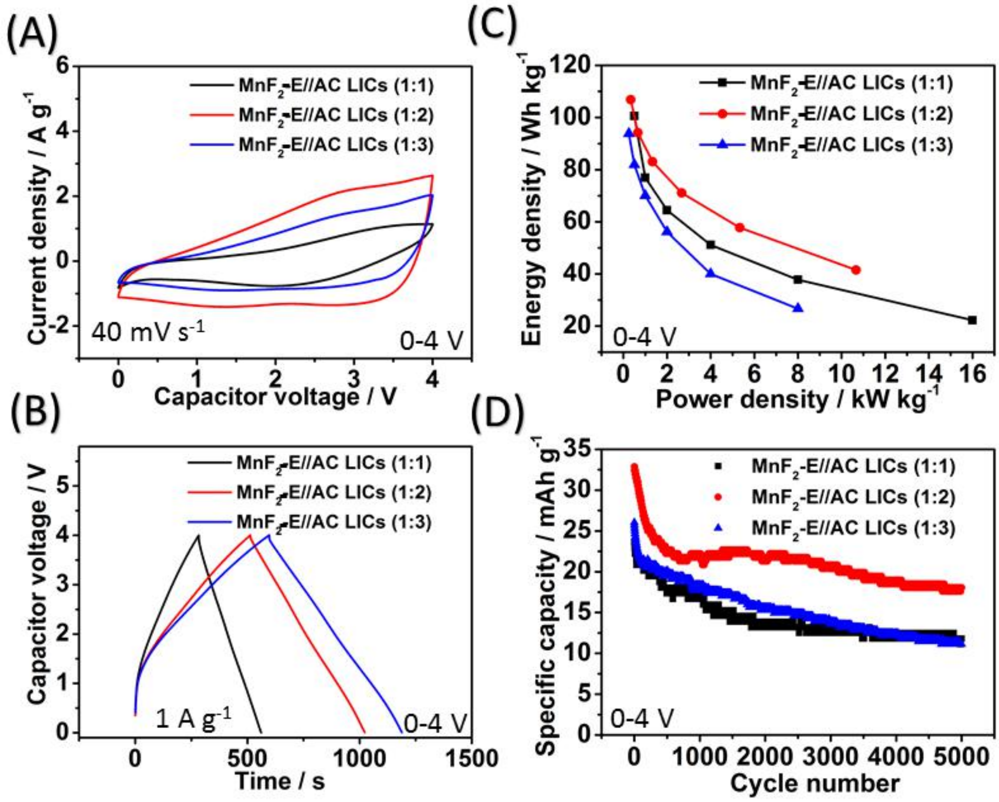

Figure S25 CV plots at 40 mV s^{-1} (A), GCD curves at 1 A g^{-1} (B), Ragone plots (C) and cycling behavior for 5000 cycles at 5 A g^{-1} (D) of 4 V-MnF$_2$//AC LICs (1:1), (1:2) and (1:3).

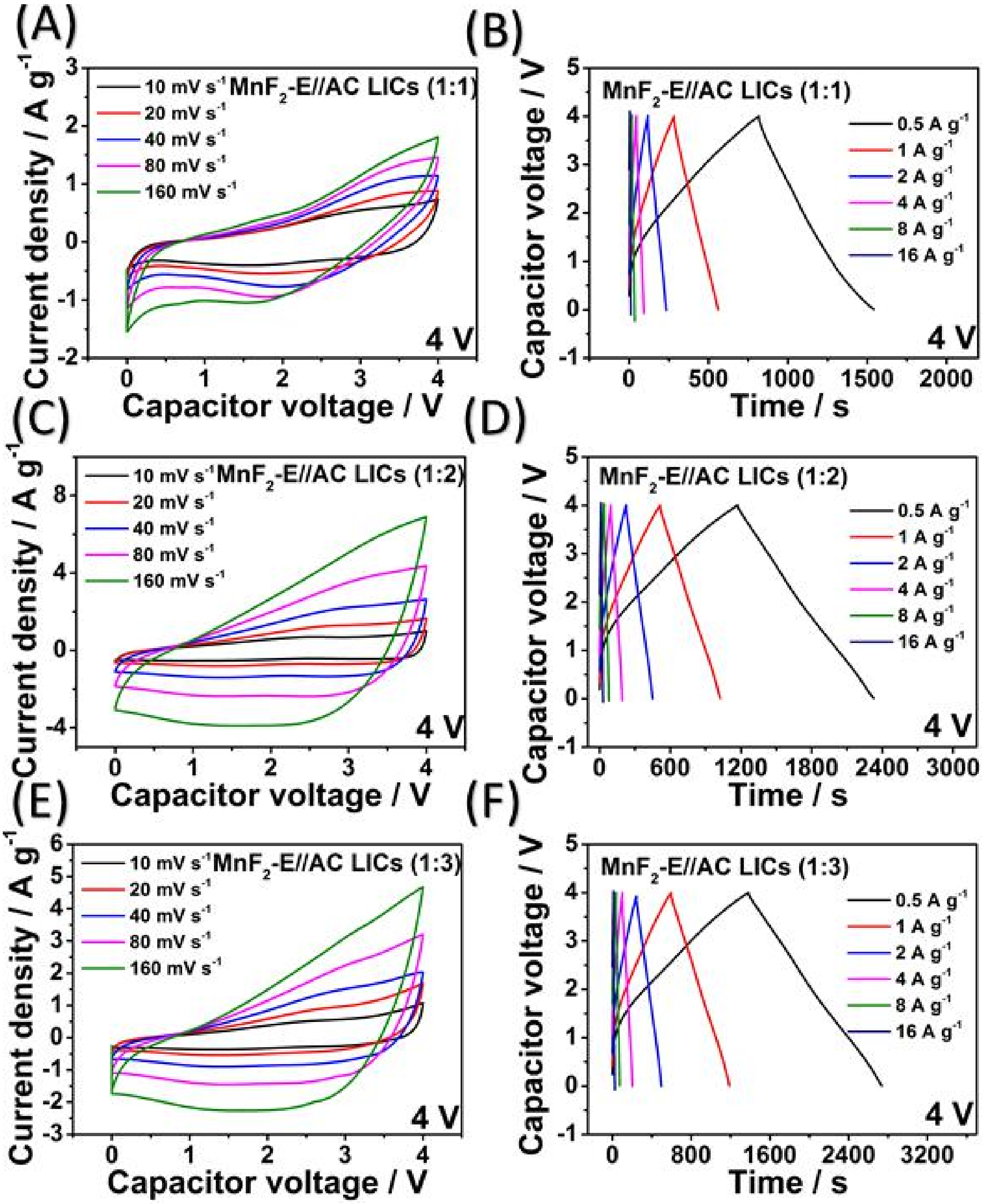

Figure S26 CV plots of 4 V-MnF$_2$-E//AC LICs (1:1) (A), 4 V-MnF$_2$-E//AC LICs (1:2) (C) and 4 V-MnF$_2$-E/AC LICs (1:3) (E) at 10-160 mV s^{-1}, GCD curves of 4 V-MnF$_2$-E//AC LICs (1:1) (B), 4 V-MnF$_2$-E//AC LICs (1:2) (D) and 4 V-MnF$_2$-E/AC LICs (1:3) (F) at 0.5-16 A g^{-1}.

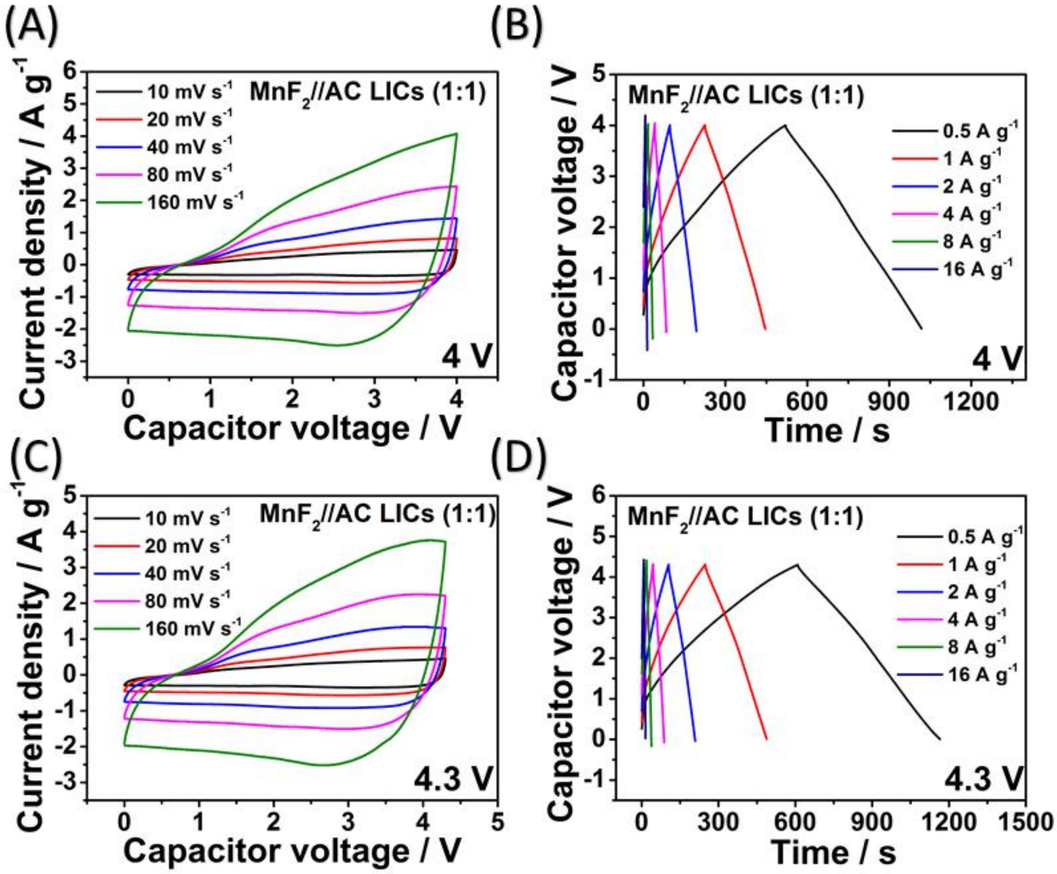

Figure S27 CV plots of 4 V-MnF_2//AC LICs (1:1) (A) and 4.3 V-MnF_2//AC LICs (1:1) (C) at 10-160 mV s^{-1}, GCD curves of 4 V-MnF_2//AC LICs (1:1) (B) and 4.3 V-MnF_2//AC LICs (1:1) (D) at 0.5-16 A g^{-1}.

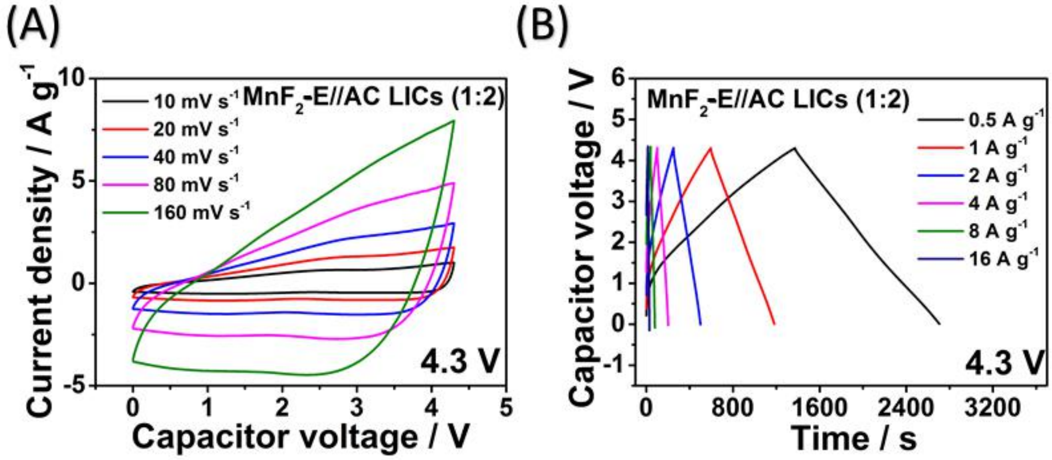

Figure S28 CV plots of 4.3 V-MnF$_2$-E//AC LICs (1:2) (A), GCD curves of 4.3 V-MnF$_2$-E//AC LICs (1:2) (B) at 0.5-16 A g^{-1}.

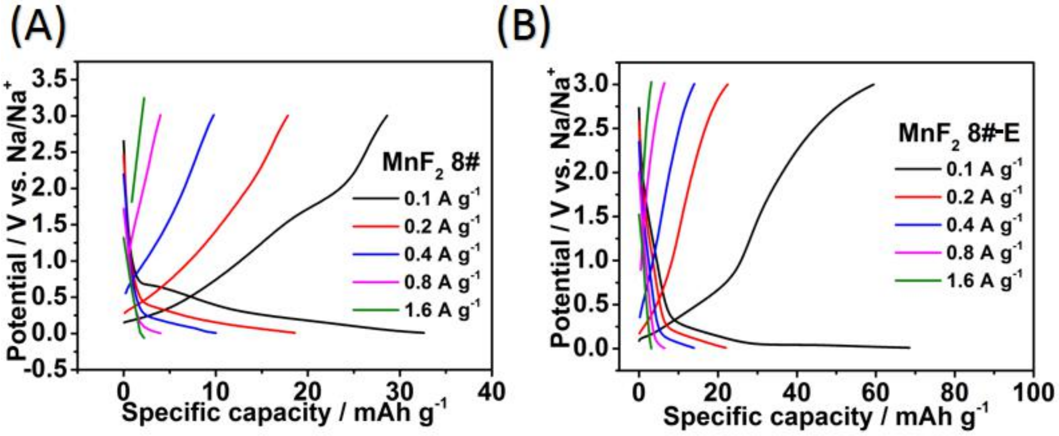

Figure S29 GCD curves of MnF_2 8# (A) and MnF_2 8#-E (B) at 0.1-1.6 A g^{-1}.

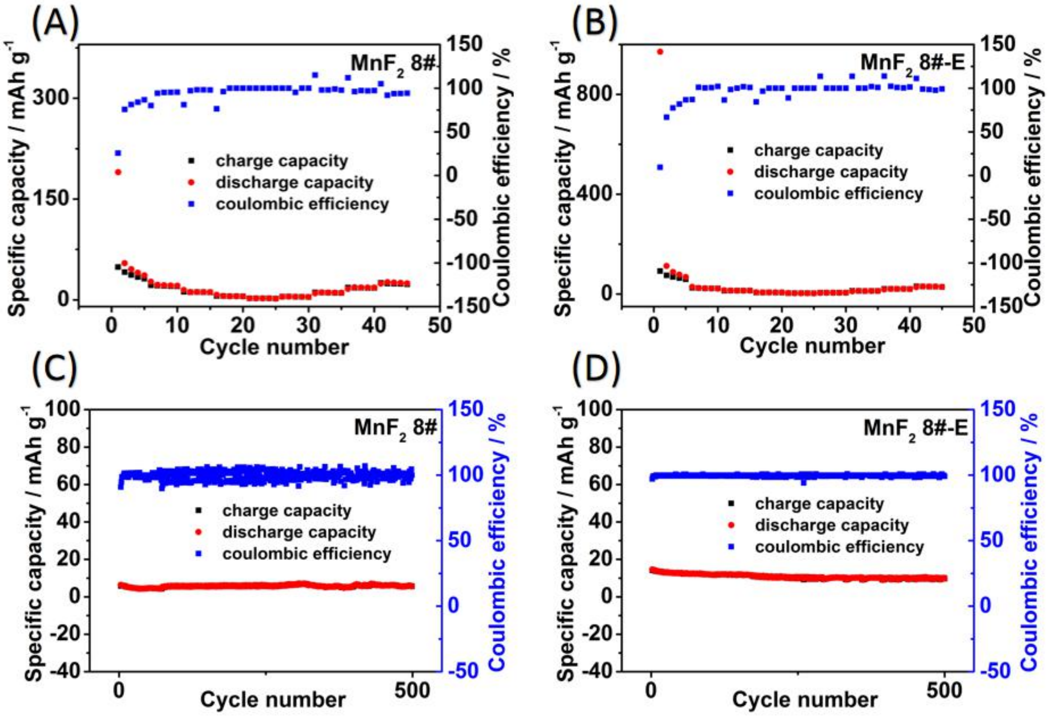

Figure S30 Rate performance and Coulombic efficiency of MnF_2 8# (A) and MnF_2 8#-E (B) electrodes at 0.1-1.6-0.1 A g^{-1}, Cycling stability and Coulombic efficiency of MnF_2 8# (C) and MnF_2 8#-E (D) electrodes at 0.3 A g^{-1} for 500 cycles.

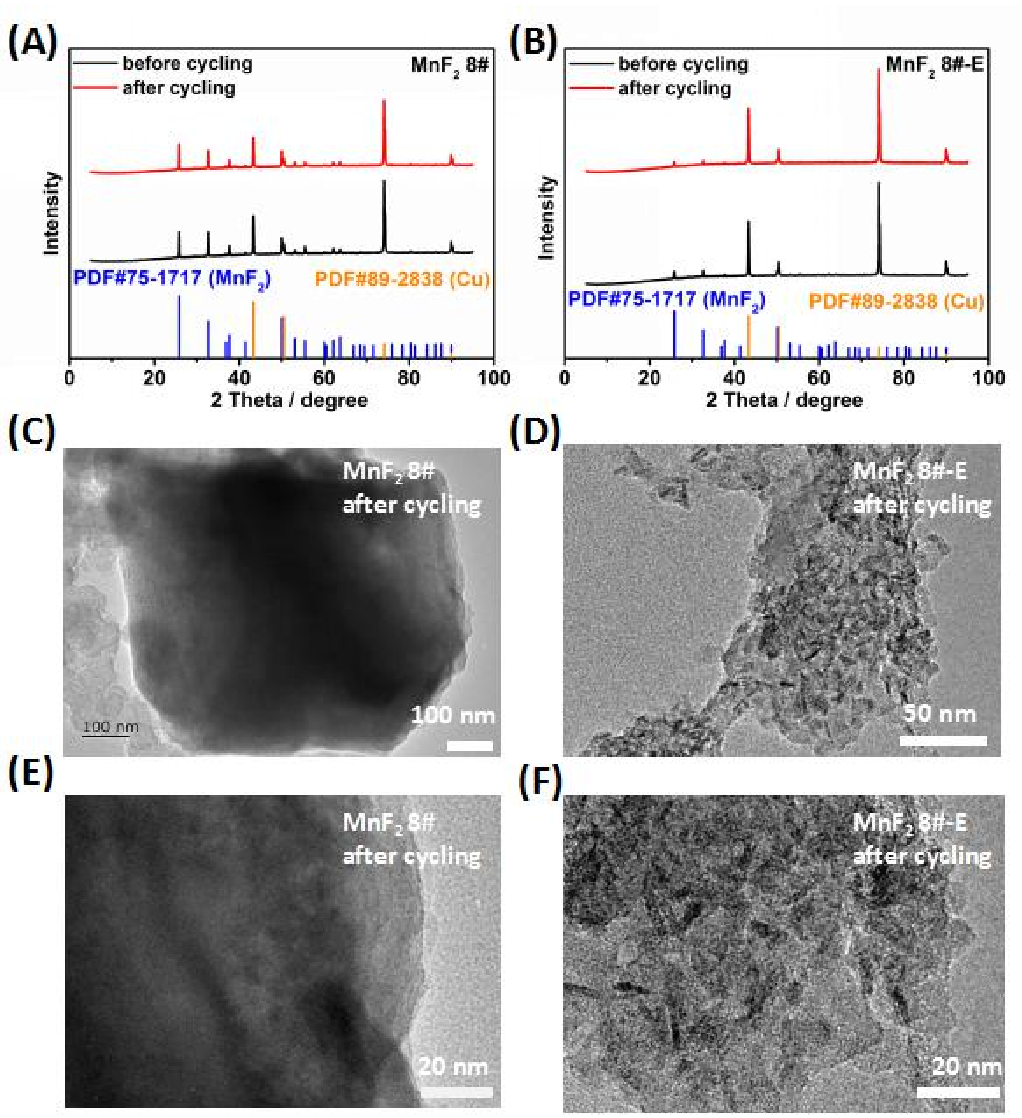

Figure S31 XRD patterns and TEM images of the MnF_2 8# (A, C, E) and MnF_2 8#-E (B, D, F) electrodes after the cycling for Na-ion storage.

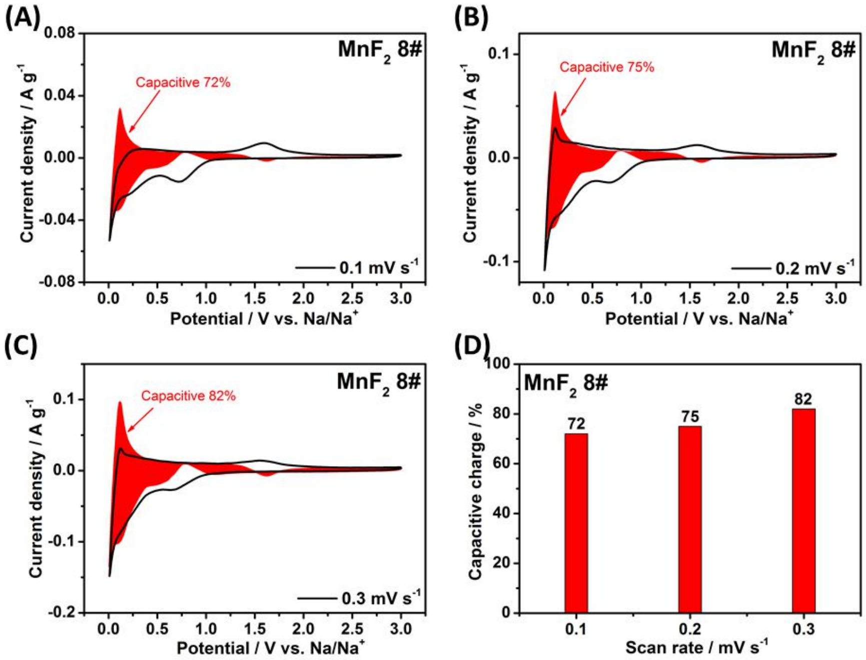

Figure S32 The pseudocapacitive contributions (the shaded region) of the MnF_2 8# electrode at 0.1-0.3 mV s^{-1} (a-c) and the contribution ratios (d) for Na-ion storage.

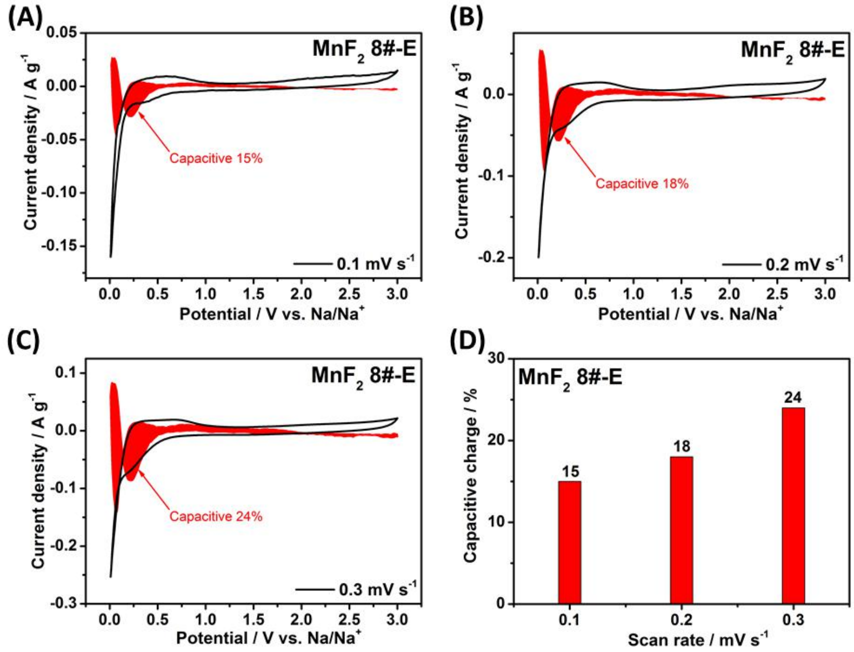

Figure S33 The pseudocapacitive contributions (the shaded region) of the MnF_2 8#-E electrode at 0.1-0.3 mV s^{-1} (a-c) and the contribution ratios (d) for Na-ion storage.

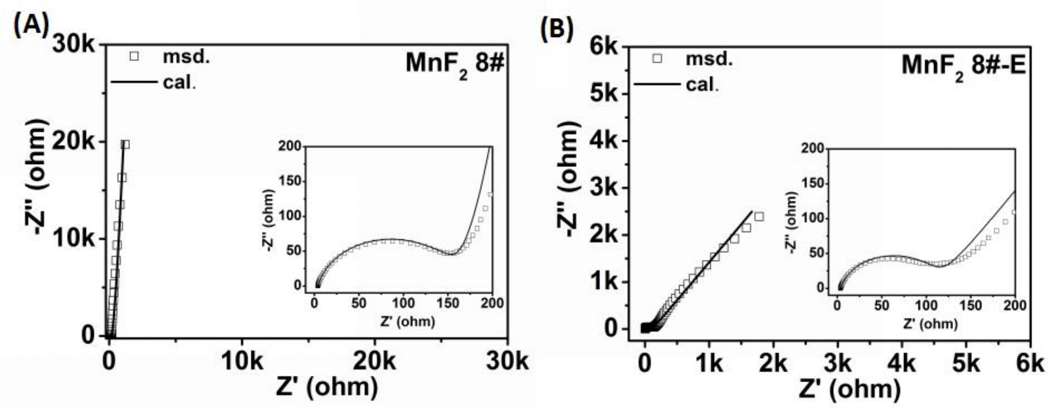

Figure S34 Nyquist plots of MnF$_2$ 8# and MnF$_2$ 8#-E electrodes (the insets are the enlarged high frequency regions).

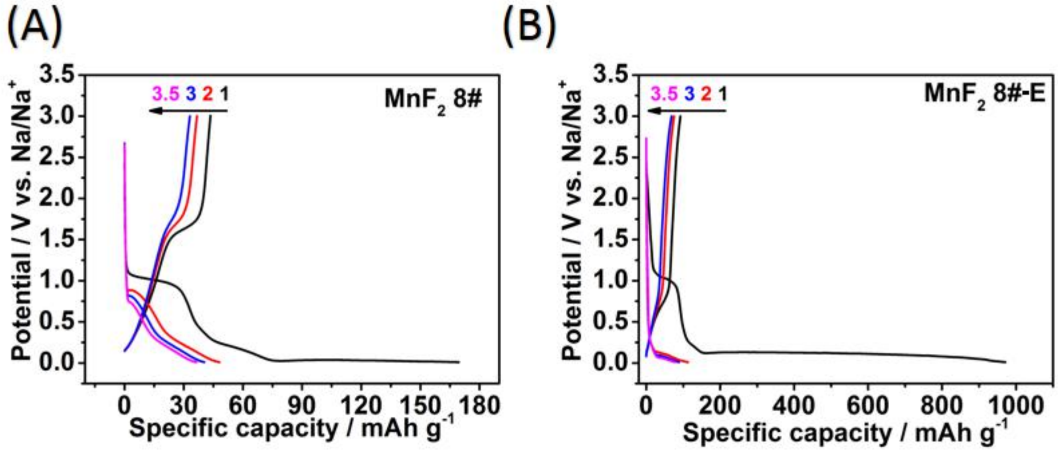

Figure S35 GCD curves of MnF_2 8# (A) and MnF_2 8#-E (B) electrodes at the precharged current density of 0.1 A g^{-1}

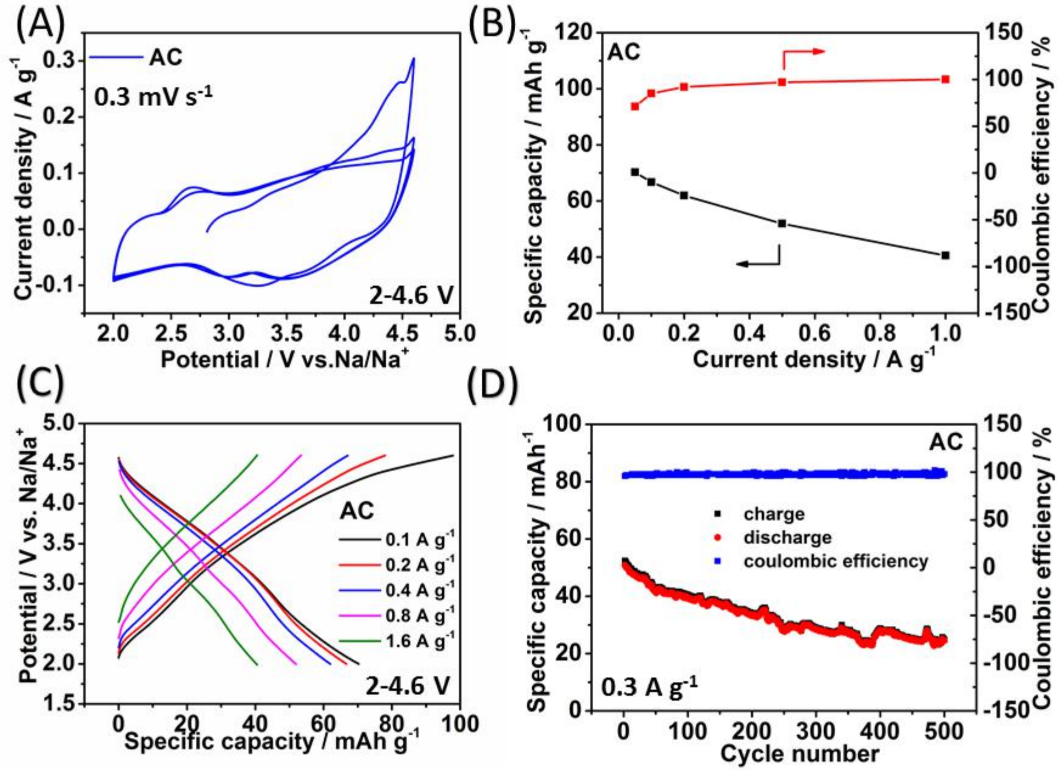

Figure S36 Performance of AC electrode for Na-ion storage.

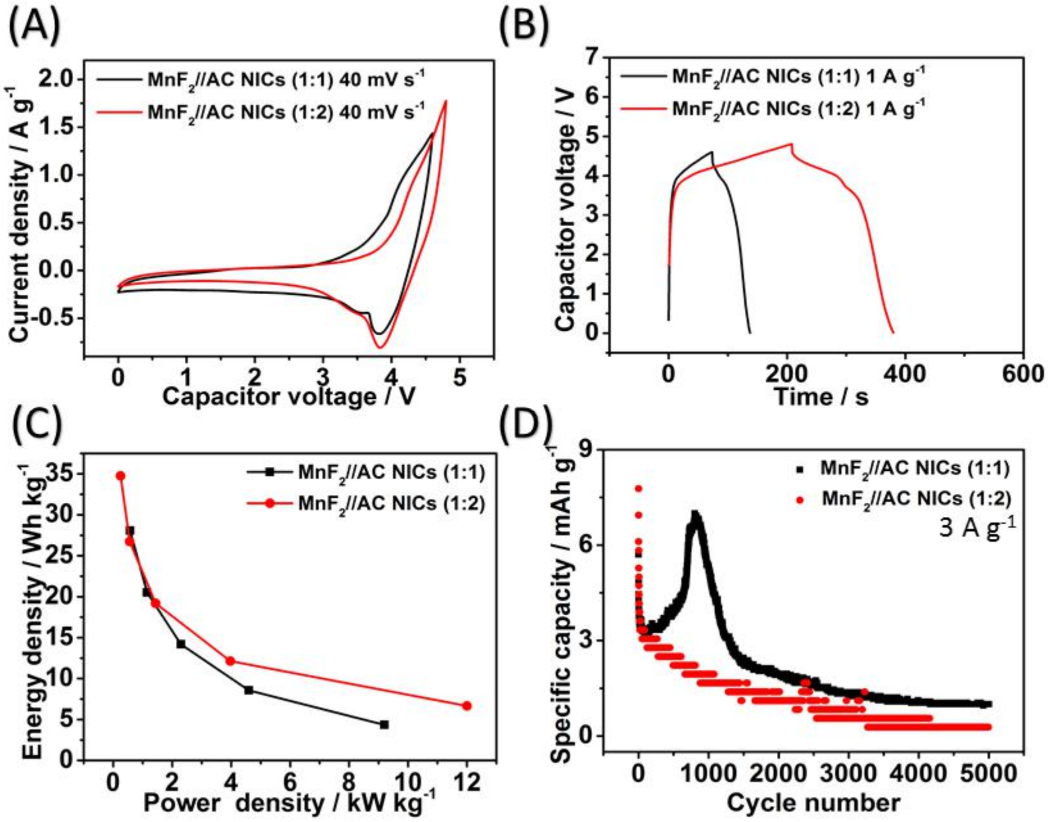

Figure S37 CV plots at 40 mV s^{-1} (A), GCD curves at 1 A g^{-1} (B), Ragone plots (C) and cycling behavior for 5000 cycles at 3 A g^{-1} (D) of 4.6 V-MnF$_2$//AC NICs (1:1) and 4.8 V-MnF$_2$//AC NICs (1:2).

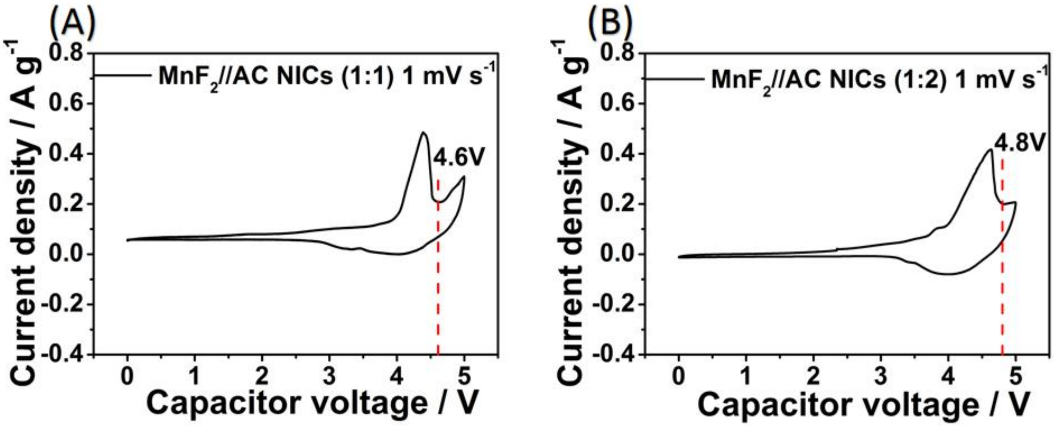

Figure S38 The third cycle CV curves at 1 mV s^{-1} under 0-5 V: MnF_2//AC NICs (1:1) (A), and MnF_2//AC NICs (1:2) (B).

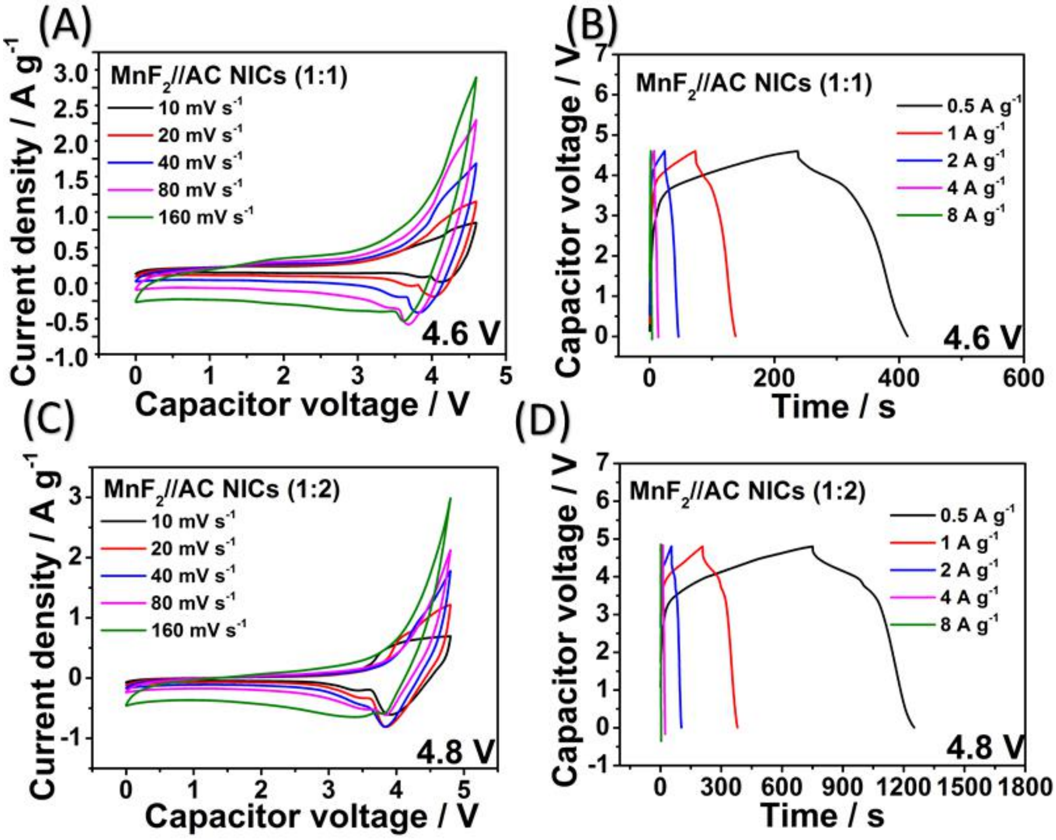

Figure S39 CV plots of 4.6 V-MnF_2//AC NICs (1:1) (A) and 4.8 V-MnF_2//AC NIC (1:2) (C) at 10-160 mV s^{-1}, GCD curves of 4.6 V-MnF_2//AC NIC (1:1) (B) and 4.8 V-MnF_2//AC NICs (1:2) (D) at 0.5-8 A g^{-1}.

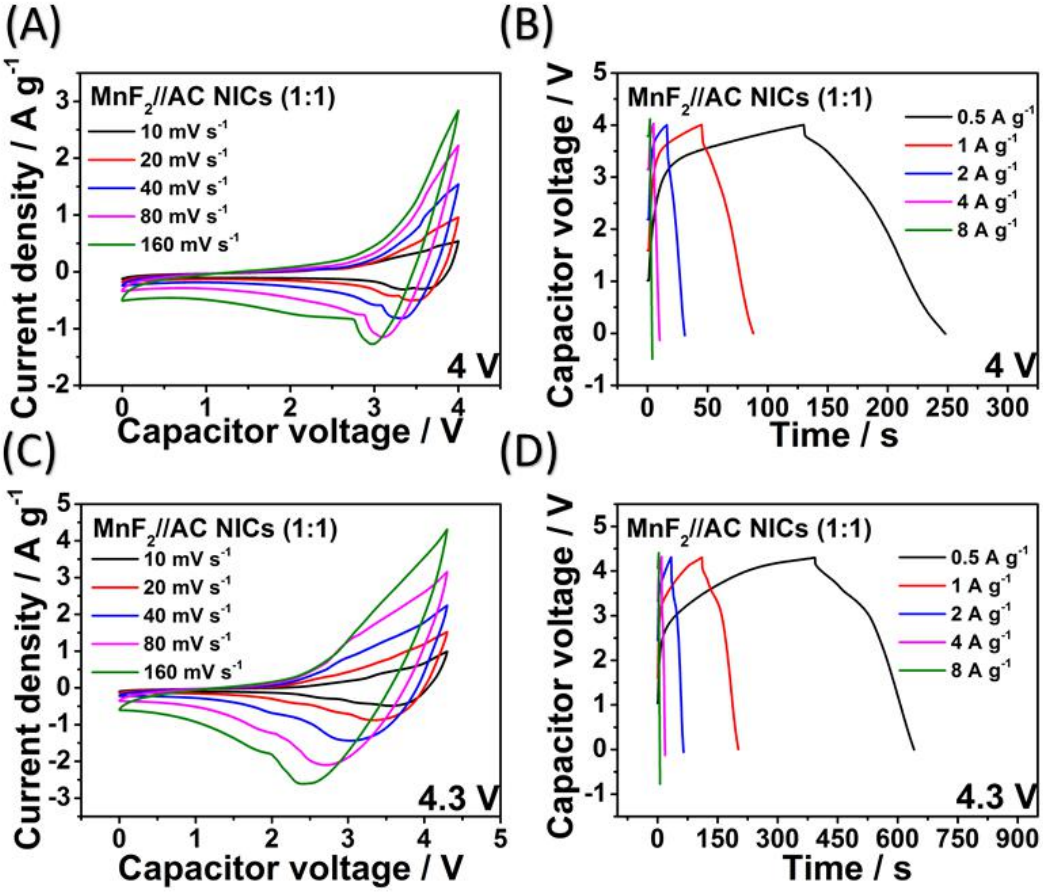

Figure S40 CV plots of 4 V-MnF_2//AC NICs (1:1) (A) and 4.3 V-MnF_2//AC NICs (1:1) (C) at 10-160 mV s^{-1}, GCD curves of 4 V-MnF_2//AC NICs (1:1) (B) and 4.3 V-MnF_2//AC NICs (1:1) (D) at 0.5-8 A g^{-1}.

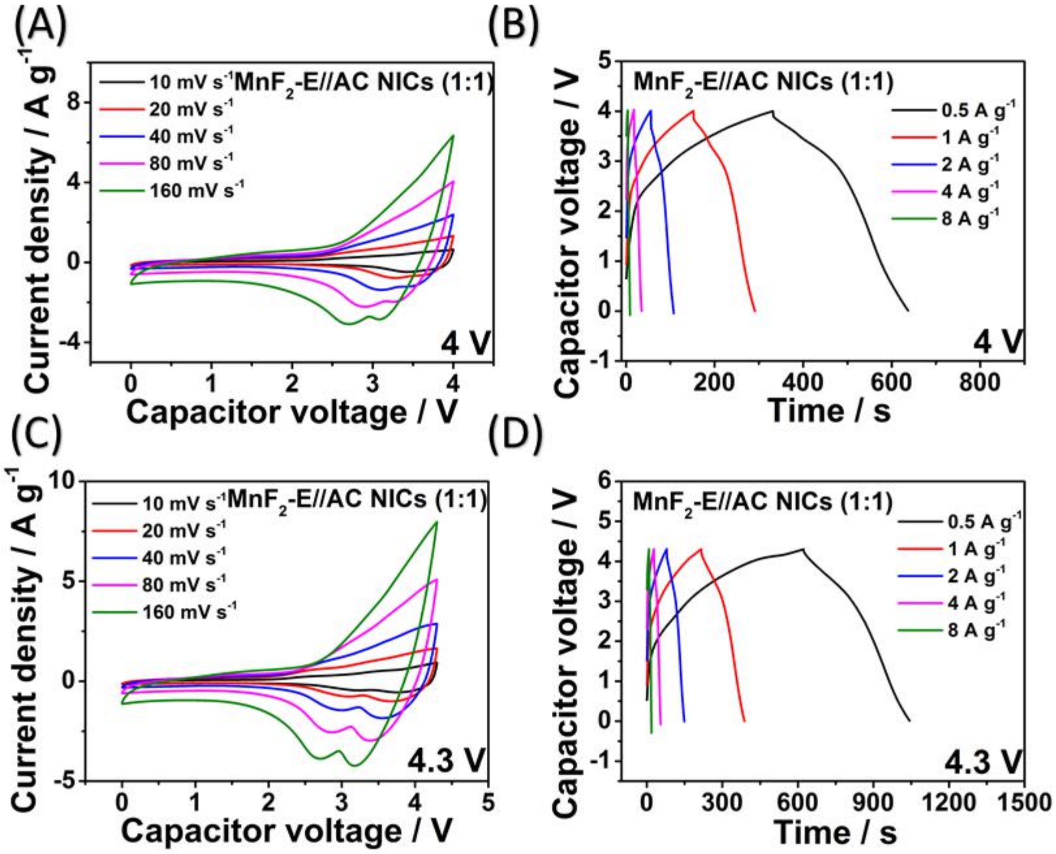

Figure S41 CV plots of 4 V-MnF_2-E//AC NICs (1:1) (A) and 4.3 V-MnF_2-E//AC NICs (1:1) (C) at 10-160 mV s^{-1}, GCD curves of 4 V-MnF_2-E//AC NICs (1:1) (B) and 4.3 V-MnF_2-E//AC NICs (1:1) (D) at 0.5-8 A g^{-1}.

Level	Factors		
	Solvent (mL)-A	Temperature (℃)-B	Time (h)-C
1	NPA	180	6
2	NBA	190	12
3	EG	200	24

Note: NPA n-propyl alcohol; NBA n-butyl alcohol; EG ethylene glycol.

Table S1 Orthogonal experimental design.

Samples	Conditions $Mn(CH_3COO)_2{\bullet}4H_2O$（mmol）	HF (40%) (mL)	Solvent (mL)	Temperature（℃）	Time（h）
1#	4	7	NPA 30	180	6
2#	4	7	NPA 30	190	12
3#	4	7	NPA 30	200	24
4#	4	7	NBA 30	180	12
5#	4	7	NBA 30	190	24
6#	4	7	NBA 30	200	6
7#	4	7	EG 30	180	24
8#	4	7	EG 30	190	6
9#	4	7	EG 30	200	12

Table S2 Synthesis condition of MnF_2 1#-9#.

Samples		**Experimental factors**			**Specific capacity (mAh g^{-1})**	**Rate retention (%)**	**Cycle retention (%)**
		A (solvent)	**B (temperature)**	**C (time)**			
1#		1（NPA）	1（180℃）	1（6h）	154	42	118
2#		1（NPA）	2（190℃）	2（12h）	163	42	153
3#		1（NPA）	3（200℃）	3（24h）	146	43	144
4#		2（NBA）	1（180℃）	2（12h）	151	49	129
5#		2（NBA）	2（190℃）	3（24h）	150	46	142
6#		2（NBA）	3（200℃）	1（6h）	149	47	145
7#		3（EG）	1（180℃）	3（24h）	143	51	147
8#		3（EG）	2（190℃）	1（6h）	162	54	141
9#		3（EG）	3（200℃）	2（12h）	144	51	145
Specific capacity（mAh/ g）	K1	463.00	448.00	465.00		MnF_2	
	K2	450.00	475.00	458.00			
	K3	449.00	439.00	439.00			
	k1	154.33	149.33	155.00			
	k2	150.00	158.33	152.67			
	k3	149.67	146.33	146.33			
	R	**4.67**	**12.00**	**8.67**			
Rate retention（%）	K1	127.00	142.00	143.00			
	K2	142.00	142.00	142.00			
	K3	156.00	141.00	140.00			
	k1	42.33	47.33	47.67			
	k2	47.33	47.33	47.33			
	k3	52.00	47.00	46.67			
	R	**9.67**	**0.33**	**1.00**			
Cycle retention（%）	K1	415.00	394.00	404.00			
	K2	416.00	436.00	427.00			
	K3	433.00	434.00	433.00			
	k1	138.33	131.33	134.67			
	k2	138.67	145.33	142.33			
	k3	144.33	144.67	144.33			
	R	**6.00**	**13.33**	**9.67**			
		Specific capacity			B>C>A	A1B2C1	
		Rate retention			A>C>B	A3(B1 or B2) C1	
		Cycle retention			B>C>A	A3B3C3	
		The optimal conditions			A3B2C3 or A3B2C1		
		Selected optimal conditions			A3B2C1		

Table S3 Orthogonal experimental analysis results of MnF_2

Devices	Samples	Specific capacity / mAh g^{-1} 0.1 (A g^{-1})	0.2 (A g^{-1})	0.4 (A g^{-1})	0.8 (A g^{-1})	1.6 (A g^{-1})	3.2 (A g^{-1})	Specific capacity after 500 cycles / mAh g^{-1}	Cycle retention / %
Li//MnF_2 LIBs	MnF_2 1#	145	128	112	94	81	65	161	168
	MnF_2 2#	149	137	125	109	89	67	123	160
	MnF_2 3#	137	130	119	104	84	68	113	153
	MnF_2 4#	145	136	125	111	94	74	109	138
	MnF_2 5#	143	132	120	105	87	70	107	153
	MnF_2 6#	143	133	125	112	97	80	128	154
	MnF_2 7#	135	125	118	106	90	74	121	151
	MnF_2 8#	**153**	**146**	**137**	**124**	**108**	**89**	**138**	**152**
	MnF_2 9#	136	127	118	106	89	74	120	154
	$MnF_2$8#-E	**411**	**346**	**285**	**235**	**179**	**120**	**271**	**207**
Na//MnF_2 NIBs	MnF_2 8#	31	19	10	4	2	-	5.4	90
	MnF_2 8#-E	59	22	14	6	4	-	11	77

Table S4 Summary of performance of MnF_2 1#-9# and MnF_2 8#-E electrodes.

Anode materials for LIBs	**Specific capacity**	**Rate behavior**	**Cycle life**	**Refs.**
MnF_2	300 mA h g^{-1} / 0.1 C	180 mA h g^{-1} / 10 C	237 mA h g^{-1} / 5000 / 10 C	***Adv. Energy Mater.***, 2015, 5, 1401716
CoF_2	350 mA h g^{-1} / 0.0553 A g^{-1}	#	13.5% / 100 / 1.1 A g^{-1}	***Electrochim. Acta***, 2015, 168, 225-233
Mn_3O_4	180 mA h g^{-1} / 0.04 A g^{-1}	#	15.9% / 50 / 0.04 A g^{-1}	***ACS Appl. Mater. Interfaces***, 2012, 4, 1636−1642
NbO_2F	250 mA h g^{-1} / 0.03 A g^{-1}	#	72% / 40/0.03A g^{-1}	***J. Power Sources***, 2006, 162, 1312–1321
Mn-O-F (MnF_2-E)	**411 mA h g^{-1} / 0.1 A g^{-1}**	**120 mA h g^{-1} / 3.2 A g^{-1}**	**271 mA h g^{-1} (207% retention) / 500 / 2 A g^{-1}**	**This work**

Table S5 A comparasion for Mn-O-F (MnF_2 8#-E) anode with literature for LIBs.

Systems (LIBs)	**Model** **$R(QR)W(QR)$**								
	R_s (Ω)	**Q_1 (S·sec^n)**	**n_1**	**R_{ct} (Ω)**	**W (S·sec$^{0.5}$)**	**Q_2 (S·sec^n)**	**n_2**	**R_e (Ω)**	**χ^2**
MnF_2 1#	3.419	4.772×10^{-4}	0.9674	**56.95**	0.03817	1.893×10^{-5}	0.8383	3.508×10^{5}	2.73×10^{-3}
MnF_2 2#	3.713	4.931×10^{-4}	0.9614	**59.62**	0.2168	1.584×10^{-5}	0.8519	1.144×10^{6}	2.1×10^{-3}
MnF_2 3#	3.372	1.508×10^{-5}	0.8458	**59.79**	0.02511	6.573×10^{-4}	0.9681	3.17×10^{6}	3.07×10^{-3}
MnF_2 4#	3.549	1.423×10^{-5}	0.8667	**62.33**	0.02601	7.544×10^{-4}	0.9733	5.186×10^{5}	2.95×10^{-3}
MnF_2 5#	3.917	8.254×10^{-4}	0.9672	**68.34**	0.02364	1.57×10^{-5}	0.8555	4.375×10^{5}	2.53×10^{-3}
MnF_2 6#	3.935	1.614×10^{-5}	0.8575	**63.11**	0.02576	7.698×10^{-4}	0.9708	5.645×10^{5}	2.43×10^{-3}
MnF_2 7#	3.34	1.395×10^{-5}	0.8741	**44.46**	0.05389	8.176×10^{-4}	0.9665	4.665×10^{5}	2.98×10^{-3}
MnF_2 8#	3.171	1.435×10^{-5}	0.8711	**46.13**	0.01497	6.862×10^{-4}	0.9751	4.267×10^{5}	2.8×10^{-3}
MnF_2 9#	3.126	5.98×10^{-4}	0.9724	**43.09**	0.02385	1.835×10^{-5}	0.8639	3.111×10^{5}	3.41×10^{-3}
MnF_2 8#-E	3.411	2.26×10^{-5}	0.8418	**37.33**	0.0168	3.506×10^{-3}	0.8056	6427	3.61×10^{-3}

Table S6 EIS parameters of MnF_2 and MnF_2 8#-E electrodes for Li-ion storage.

Systems		Voltage window	Energy density (Wh kg^{-1})			Power density (kW kg^{-1})			Cycling behavior
LICs	MnF_2//AC (1:1)	0-4.0 V	0.5 A g^{-1} 69.2	4 A g^{-1} 46.7	16 A g^{-1} 31.1	0.5 A g^{-1} 0.5	4 A g^{-1} 4.0	16 A g^{-1} 16.0	5 A g^{-1} /1000/79.4% 5 A g^{-1} /2000/79.4% 5 A g^{-1} /3000/72.5% 5 A g^{-1} /5000/72.5%
		0-4.3 V	0.5 A g^{-1} 82.9	4 A g^{-1} 52.5	16 A g^{-1} 38.2	0.5 A g^{-1} 0.54	4 A g^{-1} 4.3	16 A g^{-1} 17.2	5 A g^{-1} /1000/63.5% 5 A g^{-1} /2000/53.3% 5 A g^{-1} /3000/46.6% 5 A g^{-1} /5000/40.4%
	MnF_2 -E//AC (1:2)	0-4.0 V	0.5 A g^{-1} 106.8	4 A g^{-1} 71.1	16 A g^{-1} 41.4	0.5 A g^{-1} 0.33	4 A g^{-1} 2.7	16 A g^{-1} 10.7	5 A g^{-1} /1000/66.5% 5 A g^{-1} /2000/66.5% 5 A g^{-1} /3000/63.4% 5 A g^{-1} /5000/56.1%
		0-4.3 V	0.5 A g^{-1} 132.2	4 A g^{-1} 79.6	16 A g^{-1} 44.6	0.5 A g^{-1} 0.36	4 A g^{-1} 2.9	16 A g^{-1} 11.5	5 A g^{-1} /1000/63.5% 5 A g^{-1} /2000/60.8% 5 A g^{-1} /3000/55.1% 5 A g^{-1} /5000/47.9%
NICs	MnF_2//AC (1:1)	0-4.0 V	0.5 A g^{-1} 16.4	2 A g^{-1} 8.3	8 A g^{-1} 4.4	0.5 A g^{-1} 0.5	2 A g^{-1} 2.0	8 A g^{-1} 8.0	3 A g^{-1} /100/62.5% 3 A g^{-1} /200/50.2% 3 A g^{-1} /300/50.2% 3 A g^{-1} /40050.2% 3 A g^{-1} /500/49.8% 3 A g^{-1} /800/49.8%
		0-4.3 V	0.5 A g^{-1} 37	2 A g^{-1} 18.5	8 A g^{-1} 7.2	0.5 A g^{-1} 0.54	2 A g^{-1} 2.1	8 A g^{-1} 8.6	3 A g^{-1} /100/66.7% 3 A g^{-1} /200/66.7% 3 A g^{-1} /300/66.7% 3 A g^{-1} /400/58.4% 3 A g^{-1} /500/58.4% 3 A g^{-1} /800/58.4%
	MnF_2-E//AC (1:1)	0-4.0 V	0.5 A g^{-1} 42.1	2 A g^{-1} 28.4	8 A g^{-1} 8.9	0.5 A g^{-1} 0.5	2 A g^{-1} 2.0	8 A g^{-1} 8.0	3 A g^{-1} /100/68.4% 3 A g^{-1} /200/63.1% 3 A g^{-1} /300/52.7% 3 A g^{-1} /400/52.7% 3 A g^{-1} /500/52.7% 3 A g^{-1} /800/52.7%
		0-4.3 V	0.5 A g^{-1} 55.9	2 A g^{-1} 36.8	8 A g^{-1} 19.2	0.5 A g^{-1} 0.48	2 A g^{-1} 1.9	8 A g^{-1} 7.7	3 A g^{-1} /100/51.7% 3 A g^{-1} /200/45.3% 3 A g^{-1} /300/41.9% 3 A g^{-1} /400/35.4% 3 A g^{-1} /500/35.4% 3 A g^{-1} /800/32.2%

Table S7 Summary of performance of MnF_2//AC and MnF_2-E//AC LICs and NICs.

Systems	Voltage window / V	Energy density / Wh kg^{-1}	Power density / kW kg^{-1}	Cycling behavior / retention%, repeated cycles, current density	Refs.
$TiSe_{0.6}S_{1.4}$//AC	0-2.6	50-14	-	69%/5000/ 1 A g^{-1}	**1**
TiO_2-rGO//AC	1.0-4.5	42-8.9	0.8-8.0	80%/100/ 0.4 Ag^{-1}	**2**
CNT/V_2O_5//AC	1.8-4.0	25.5-6.9	0.04-6.3	-	**3**
TiO_2 -B//CNT	0.0-2.8	23-7	0.14-2.8	73%/1200/ 1.5 A g^{-1}	**4**
TiO_2 belt///graphene	0.0-3.8	82-21	0.57-19	73%/600/ 1 A g^{-1}	**5**
TiO_2@EEG//EEG	0.0-3.0	72-10	0.303-2.0	68%/1000/ 1.5 A g^{-1}	**6**
MnF_2 8#//AC (1:1)	**0-4.0**	**69.2-31.1**	**0.5-16.0**	**72.5%/5000/ 5 A g^{-1}**	**This work**
	0-4.3	**82.9-38.2**	**0.54-17.2**	**63.5%/1000/ 5 A g^{-1}**	
MnF_2 8#-E//AC (1:2)	**0-4.0**	**106.8-41.4**	**0.33-10.7**	**63.4%/3000/ 5 A g^{-1}**	
	0-4.3	**132.2-44.6**	**0.36-11.5**	**60.8%/2000/ 5 A g^{-1}**	

Note: EEG   graphene nanosheets; CNT   carbon nanotube;   rGO   Reduced Graphene Oxide

Table S8 Electrochemical performance comparison for some reported LICs.

Systems (NIBs)	**Model $R(QR)W(QR)$**								
	R_s (Ω)	**Q_1 (S·sec^n)**	**n_1**	**R_{ct} (Ω)**	**W (S·sec$^{0.5}$)**	**Q_2 (S·sec^n)**	**n_2**	**R_e (Ω)**	**χ^2**
MnF_2 8#	3.68	6.526×10^{-4}	0.9872	**144.8**	0.004796	1.366×10^{-5}	0.8916	2.154×10^{14}	3.26×10^{-3}
MnF_2 8#-E	3.632	1.468×10^{-5}	0.8627	**106.7**	8.269×10^{7}	1.775×10^{-3}	0.6392	4.173×10^{11}	4.23×10^{-3}

Table S9 EIS parameters of MnF_2 8# and MnF_2 8#-E electrodes for Na-ion storage.

Systems	Voltage window / V	Energy density / Wh kg^{-1}	Power density / kW kg^{-1}	Cycling behavior / retention%, repeated cycles, current density	Refs.
$NiCo_2O_4$//AC	0-3.0	23.5-13.8	0.036-0.308	61.2%/2000/ 0.15 A g^{-1}	**7**
$Na_{0.44}MnO_2$ // $Na_{0.44}MnO_2$	0-1.6	27.9-15	0.012-0.24	-	**8**
V_2O_5/CNT//AC	0-2.8	38-7.5	0.14-5.0	-	**9**
Na-TNT//AC	0-3.0	34-13	0.15-0.89	80%/1000/ 0.25 A g^{-1}	**10**
MnF_2 8#//AC (1:1)	**0-4.3**	**37-7.2**	**0.54-8.6**	**66.7%/100/ 3 A g$^{-1\#}$** **66.7%/300/ 3 A g$^{-1\#}$** **58.4%/500/ 3 A g$^{-1\#}$** **58.4%/800/ 3 A g$^{-1\#}$** **88.8%/100/ 3 A g^{-1*}** **88.8%/300/ 3 A g^{-1*}** **77.9%/500/ 3 A g^{-1*}** **77.9%/800/ 3 A g^{-1*}**	**This work**
MnF_2 8#-E//AC (1:1)	**0-4.0**	**42.1-8.9**	**0.5-8.0**	**68.4%/100/ 3 A g$^{-1\#}$** **63.1%/200/ 3 A g$^{-1\#}$** **52.7%/500/ 3 A g$^{-1\#}$** **52.7%/800/ 3 A g$^{-1\#}$** **86.7%/100/ 3 A g$^{-1@}$** **80.0%/200/ 3 A g$^{-1@}$** **67.2%/500/ 3 A g$^{-1@}$** **67.2%/800/ 3 A g$^{-1@}$**	

Note: # Based on the 1st cycle; * Based on the 5th cycle; @ Based on the 20th cycle

Table S10 Electrochemical performance comparison for some reported NICs.

Chemials, agents and materials	Type or level	Company	Detailed characteristics or parameters
$Mn(CH_3COO)_2 \cdot 4H_2O$	AR	SinoPharm	purity≥99.0%
HF	AR	Zhanyun	purity≥40.0%
EG	AR	SinoPharm	purity≥99.0%
NPA	AR	SinoPharm	purity≥99.0%
NBA	AR	SinoPharm	purity≥99.0%
NMP	AR	SinoPharm	purity≥99.0%
$NaBH_4$	AR	SinoPharm	purity≥96.0%
AB	Battery grade	/	/
PVDF	Battery grade	/	/
Li plate	Battery grade	China Energy	15.6*0.45 mm
Na plate	Battery grade	/	/
Cu foil	200*0.015	GuangZhou JiaYuan	Total thickness: 15 μm; weight: 87 g m^{-2}
Carbon coated-Al foil	222*0.015	GuagZhou NaNuo	Total thickness: 17 μm; Strength: 192 Mpa
Glass microfiber filters	GF/D 2.7 μm; 1823-025	Whatman	Diameter: 25 mm; Thickness: 675 μm; weight: 121 g m^{-2}
AC	YEC 8b	Fuzhou YiHuan	D50: ~10 μm; Density: 0.4 g cm^{-3} ; SSA:2000~2500 m^2 g^{-1}
Li-ion electrolytes	LBC-305-01	CAPCHEM	1 M $LiPF_6$ /EC:EMC:DMC (1:1:1) /1% VC
Na-ion electrolytes	/	MJS	0.85 M $NaPF_6$ /EC:DEC (1:1) / 5% FEC
Cell components	CR-2032	Shenzhen TianChenHe	/

Table S11 Chemicals, agents and materials.

References

1. A. Chaturvedi, P. Hu, C. Kloc, Y. S. Lee,V. Aravindan and S. Madhavi, *J. Mater. Chem. A,* 2017, **5**, 19819-19825.
2. H. Kim , M. Y. Cho , M. H. Kim , K. Y. Park , H. Gwon, Y. Lee , K. C. Roh and K. Kang, *Adv. Energy Mater.,* 2013, **3**, 1500.
3. Z. Chen,V. Augustyn, J. Wen ,Y. W. Zhang ,M. Q. Shen ,B. Dunn and Y. F. Lu, *Adv. Mater.,* 2011, **23**, 791.
4. V. Aravindan, N. Shubha, W. C. Ling and S. Madhavi, *J. Mater. Chem. A,* 2013, **1**, 6145-6151.
5. H. W. Wang, C. Guan, X. F. Wang and H. J. Fan, *Small,* 2015, **11**, 1470-1477.
6. F. X. Wang, C. Wang, Y. J. Zhao, Z. C. Liu, Z. Chang, L. J. Fu, Y. S. Zhu, Y. P. Wu and D. Y. Zhao, *Small*, 2016, **12**, 6207-6213.
7. R. Ding, L. Qi and H. Y. Wang, *Electrochim. Acta,* 2013, **114**, 726-735.
8. Z. X. Chen, T. C. Yuan, X. J. Pu, H. X. Yang, X. P. Ai, Y. Y. Xia and Y. L. Cao, *ACS Appl. Mater. Interfaces,* 2018, **10**, 11689-11698.
9. Z. Chen, V. Augustyn, X. L. Jia, Q. F. Xiao, B. Dunn and Y. F. Lu, *ACS Nano,* 2012, **6**, 4319-4327.
10. J. Yin, L. Qi and H. Y. Wang, *ACS Appl. Mater. Interfaces,* 2012, **4**, 2762-2768.